LKB1 depletion-mediated epithelial–mesenchymal transition induces fibroblast activation in lung fibrosis

Zijian Xu[1,*], Elizabeth R. Davies[1,2,*], Liudi Yao[1], Yilu Zhou[1,3], Juanjuan Li[1], Aiman Alzetani[4,5], Ben G. Marshall[4,5], David Hancock[6], Tim Wallis[4,5], Julian Downward[6], Rob M. Ewing[1,3], Donna E. Davies[2,3,4], Mark G. Jones[2,3,4,#], and Yihua Wang[1,3,4,#]

[1]Biological Sciences, Faculty of Environmental and Life Sciences, University of Southampton, Southampton SO17 1BJ, UK. [2]Clinical and Experimental Sciences, Faculty of Medicine, University of Southampton, Southampton SO16 6YD, UK. [3]Institute for Life Sciences, University of Southampton, Southampton SO17 1BJ, UK. [4]NIHR Southampton Biomedical Research Centre, University Hospital Southampton, Southampton SO16 6YD, UK. [5]University Hospital Southampton, Southampton SO16 6YD, UK. [6]Oncogene Biology, The Francis Crick Institute, London NW1 1AT, UK.

[*]These authors contributed equally.

[#]Correspondence should be addressed to YW (e-mail: yihua.wang@soton.ac.uk) or MGJ (mark.jones@soton.ac.uk).

Running title: LKB1 inhibition in pulmonary fibrosis

Abstract

The factors that determine fibrosis progression or normal tissue repair are largely unknown. We previously demonstrated that autophagy inhibition-mediated epithelial-mesenchymal transition (EMT) in human alveolar epithelial type II (ATII) cells augments local myofibroblast differentiation in pulmonary fibrosis by paracrine signalling. Here, we report that liver kinase B1 (LKB1) inactivation in ATII cells inhibits autophagy and induces EMT as a consequence. In IPF lungs, this is caused by downregulation of *CAB39L*, a key subunit within the LKB1 complex. 3D co-cultures of ATII cells and MRC5 lung fibroblasts coupled with RNA sequencing (RNA-seq) confirmed that paracrine signalling between LKB1-depleted ATII cells and fibroblasts augmented myofibroblast differentiation. Together these data suggest that reduced autophagy caused by LKB1 inhibition can induce EMT in ATII cells and contribute to fibrosis via aberrant epithelial–fibroblast crosstalk.

Introduction

Idiopathic pulmonary fibrosis (IPF) is a chronic, progressive, fibrotic lung disease of unknown aetiology [1]. In IPF the current paradigm of disease pathogenesis proposes that the delicate alveolar architecture of the lung is disrupted by extracellular matrix (ECM) deposition as a consequence of repetitive micro-injuries to the alveolar epithelium, resulting in tissue scarring, increased stiffness and impaired gas exchange. Two anti-fibrotic drugs, nintedanib and pirfenidone, are approved worldwide for the treatment of IPF however whilst there is evidence that they can slow disease progression they cannot stop or reverse it [2] and so better treatments are urgently required.

We previously identified that alveolar epithelial type II (ATII) cells undergoing epithelial-mesenchymal transition (EMT) promote a pro-fibrotic microenvironment through paracrine signalling activating local fibroblasts [3, 4, 5]. EMT is a dynamic, reversible process which has been implicated in embryonic development, wound healing, cancer metastasis and fibrosis [6]. Induction of EMT in fibrosis has been linked to a variety of processes including autophagy inhibition which triggers EMT via the p62/*SQSMT1*-NFκB-Snail2 signalling pathway [3, 7]. Autophagy (macro-autophagy) is a regulated self-management mechanism allowing the bulk or selective degradation of intracellular components and has been widely associated with several ageing processes including neurodegeneration, cancer and fibrosis [8]. It has been reported that autophagy activity is reduced in IPF [9, 10, 11, 12, 13], however, signalling pathways leading to this phenomenon remain to be elucidated. Here, we report that inactivation of Liver Kinase B1 (LKB1, encoded by the gene *Serine/Threonine Kinase 11*, *STK11*) in ATII cells inhibits autophagy and induces EMT. We identified downregulation of *CAB39L*, the allosteric activator of LKB1 in IPF alveolar septae and found that levels of *CAB39L* were significantly inversely correlated with *SNAI2* (Snail2) suggesting that reduction

of *CAB39L* in IPF alveolar epithelium leads to LKB1 inactivation and promotes EMT. The profibrotic relevance of alveolar LKB1 inactivation was demonstrated in 3D co-cultures of ATII cells and lung fibroblasts in which paracrine signalling between LKB1-depleted ATII cells and fibroblasts was shown to augment myofibroblast differentiation.

Results

Global transcriptomic changes in LKB1-depleted alveolar type II (ATII) cells.

It was reported previously that activation of AMP-activated protein kinase (AMPK), a downstream effector of LKB1, in myofibroblasts from IPF lungs reduces fibrogenic activity [14]. To determine if, and how, ATII cells responded to alteration of LKB1 activity, we characterized the global transcriptomic changes in ATII cells upon RNA interference (RNAi)-mediated LKB1 depletion by performing RNA-seq. The human ATII cell line grows in continuous culture and expresses the ATII cell marker, pro-surfactant protein C, as reported earlier [7].

Differentially expressed genes (DEGs) were defined by a false discovery rate (FDR)-adjusted *P* value (P_{adj}) less than 0.05 and $|Log_2FoldChange|$ above 1. In total, 763 up-regulated and 664 down-regulated DEGs were identified (Table S1). Gene Ontology (GO) enrichment analysis was performed and grouped into molecular function, biological process and cellular component. Of note, several EMT-related terms were identified, including cell junction, chemotaxis and regulation of cell migration (FDR < 0.05; Figs. 1A and S1; Table S2). To provide further mechanistic insights, Gene Set Enrichment Analysis (GSEA) [15] was performed and several Hallmark pathways were identified, including "TNFα signalling pathway via NFκB" and "EMT" as top up-regulated pathways in LKB1-depleted ATII cells (Fig 1B; Table S3).

LKB1 depletion in ATII cells induces EMT.

Given that the "Hallmark_EMT" pathway was positively enriched upon LKB1 (*STK11*) depletion in ATII cells (Fig. 2A; normalized enrichment score, NES = 2.03; FDR < 0.001), we examined changes in EMT-associated genes. We identified increases in expression of *VIM* (Vimentin, a mesenchymal marker) and several EMT-transcriptional factors, in particular

SNAI2 (encoding Snail2), as well as a reduction in *CDH1* (encoding E-cadherin, an epithelial marker) in our RNA-seq dataset (Fig. 2B) which we confirmed by real time qPCR (Fig. 2C), as well as demonstrating increased protein levels of Snail2 while E-cadherin protein was decreased (Fig. 2D). Together, these results demonstrate that loss of LKB1 activates an EMT programme in ATII cells.

LKB1 depletion leads to autophagy inhibition-mediated EMT via the p62-NFκB-Snail2 pathway in ATII cells.

Another highly enriched pathway in LKB1-depleted ATII cells was "Hallmark_TNFα signalling pathway via NFκB" (Fig. S2A; normalized enrichment score, NES = 2.45; FDR < 0.001). To verify this, we assessed NFκB activity using a reporter assay identifying that LKB1 depletion in ATII cells increased NFκB activity above 2-fold (Fig. S2B; $P < 0.01$).

We have previously demonstrated that autophagy inhibition induced accumulation of p62/*SQSMT1* and activation of the NFκB pathway [3, 16] . Given our identification of increased NFκB activity upon LKB1 silencing, we therefore investigated the role of LKB1 on autophagy activity in ATII cells. This identified that LKB1 depletion in ATII cells led to autophagy inhibition, as demonstrated by decreased levels of LC3-II and increased p62 by western blot analysis (Fig. 3A), as well as punctate staining for p62 by immunofluorescence (Fig. 3B).

We next checked if LKB1 depletion induced EMT via the p62-NFκB-Snail2 pathway. Depletion of p62 abolished the increase in NFκB activity induced by LKB1 knockdown (Fig. 3C), suggesting that LKB1 depletion in ATII cells triggers the NFκB pathway via p62. Functionally, knockdown of either NFκB p65 (Fig. 3D) or p62 (Fig. 3E) abolished the increase in Snail2 expression induced by LKB1 depletion in ATII cells. Taken together, these results

demonstrate that LKB1 inactivation in ATII cells inhibits autophagy and promotes EMT via a p62-NFκB pathway.

Down-regulation of *CAB39L* in human IPF lungs.

Activation of LKB1 occurs via allosteric binding of LKB1 to STE20-related adaptor (*STRAD*) and mouse protein 25 (MO25, encoded by *CAB39* and *CAB39L*) [17]. Given our *in vitro* findings, we compared the expression of LKB1 (*STK11*), *STRADA*, *STRADB*, *CAB39* and *CAB39L* in IPF and control lungs in a transcriptomic dataset that we have recently established (GSE169500) [18]. Briefly, laser capture microdissection was performed upon Formalin-Fixed Paraffin-Embedded (FFPE) control non-fibrotic lung tissue (alveolar septae, n = 10) and usual interstitial pneumonia/idiopathic pulmonary fibrosis FFPE lung tissue (fibroblast foci and adjacent non-affected alveolar septae, n = 10 each), followed by RNA-seq. Among those subunits within the LKB1 complex, only the expression of *CAB39L*, the allosteric activator of LKB1, was down-regulated in IPF alveolar septae (Fig. 4A). By contrast, expression of other subunits, including LKB1 (*STK11)*, *STRADA*, *STRADB* and *CAB39*, did not significantly change in IPF lungs (Fig. S3). Down-regulation of *CAB39L* in human IPF lung tissue was confirmed using real time qPCR of IPF tissue lysates (Fig. 4B; $P < 0.05$) as well as RNA *in situ* hybridisation of alveolar septae (Fig. 4C). We also assessed the expression of *CAB39L* and *SNAI2* (encoding Snail2) in alveolar septae from control and IPF lungs using the same dataset (GSE169500) and found that the levels of *CAB39L* were significantly inversely correlated with *SNAI2* (Snail2) (Fig. 4D, Pearson $r = -0.65$; $n = 20$; $P = 0.002$). These observations support the concept that in IPF alveolar epithelium down-regulation of *CAB39L* leads to LKB1 inactivation and promotes EMT via the p62-NFκB pathway (Fig. 4E).

3D co-cultures of ATII cells and pulmonary fibroblasts suggest involvement of paracrine signalling in augmenting myofibroblast differentiation.

Our previous study reported that reduced autophagy activity contributed to fibrosis via aberrant epithelial-fibroblast crosstalk [3]. To determine if it was also the case for LKB1-depletion in ATII cells, 2D cultures of ATII cells alone or 3D co-cultures with MRC5 lung fibroblasts (Fig. 5A) were established and then analysed by RNA-seq. DEGs were defined by a FDR-adjusted *P* value (P_{adj}) less than 0.05 and |Log_2FoldChange| above 1 (Table S4).

Our earlier reports [3, 5] by comparison of the relative expression of ECM components in ATII cells and fibroblasts highlight that ATII cells produce extremely low levels of ECM genes even after the induction of EMT, suggesting that ECM production in fibrosis is more likely to be a consequence of fibroblast activation than direct deposition by epithelial cells undergoing EMT. This is also true in this study. A comparison of collagen genes in 2D monocultures of control or LKB1-depleted ATII showed relatively low levels of collagen gene expression that were not significantly different (control ATII *vs.* LKB1-depleted ATII; Fig. 5B; Table S5), even though an EMT signature was clearly detectable in the LKB1 depleted cells (Figs. 1 and 2). In contrast, when LKB1-depleted ATII cells were co-cultured with MRC5 fibroblasts, there was a marked up-regulation of a large number of collagen genes (control ATII + MRC5 *vs.* LKB1-depleted ATII + MRC5; Fig. 5B; Table S5). Quantification of the changes in collagen gene expression using Gene Set Variation Analysis (GSVA) [19], identified a significant effect of LKB1 depletion in 3D co-cultures of ATII cells and MRC5 (Fig. 5C; $P < 0.01$), but not in 2D-cultured ATII cells (Fig. 5C; $P > 0.05$). This suggested collagen production in IPF lungs is unlikely to be a direct consequence of epithelial collagen gene expression due to EMT, but rather epithelial

155 cells exhibiting an indirect effect on fibroblast differentiation via paracrine signalling,
156 especially when undergoing EMT [3, 5].

157 To further explore the effect of paracrine signalling on fibroblast to myofibroblast transition,
158 in 3D co-cultures we analysed the expression of *ACTA2* (α-SMA, a myofibroblast marker),
159 confirming that LKB1 depletion in ATII cells caused increased expression and that this was
160 associated with up-regulations in *COL1A1*, *COL3A1*, and *FN1* (Fig. 5D; all *P values* < 0.01).
161 Finally, to confirm the paracrine influence of ATII cells on fibroblast differentiation, we treated
162 MRC5 cells with conditioned media (CM) from ATII cells transfected with control or LKB1
163 siRNA without or with addition of transforming growth factor-β (TGF-β), and assessed levels
164 of α-SMA. CM from ATII cells transfected with LKB1 siRNA without TGF-β had a similar
165 effect on α-SMA expression compared to TGF-β treatment alone (Fig. 5E). Furthermore, CM
166 from LKB1-depleted ATII cells together with TGF-β achieved a strong synergistic effect on
167 α-SMA protein levels (Fig. 5E). These data suggest that LKB1 depletion in ATII cells
168 augments myofibroblast differentiation via paracrine signalling.

Discussion

IPF is a progressive interstitial lung disease with limited treatment options available [20]. Although the underlying cause of IPF is not fully understood, repetitive microinjuries to aged alveolar epithelium is proposed to trigger aberrant wound healing processes, initiating an accumulation of ECM deposited by myofibroblasts [21], which are critical in the pathogenesis of IPF, with increased fibroblast foci associated with worse prognosis [22]. The origin of myofibroblasts in IPF is controversial and it was proposed that ATII cells undergoing EMT may be a source of myofibroblasts in fibrotic diseases. However, findings from our group suggest that ATII cells undergoing EMT induced by RAS activation [5] or autophagy inhibition [3] express only low levels of ECM genes. Our findings in this study support the concept that epithelial cells do not directly contribute to myofibroblast populations via EMT, rather they are able to promote myofibroblast differentiation through paracrine signaling [7].

LKB1 is an evolutionarily conserved serine/threonine protein kinase, which acts as an important regulator of cell polarity, proliferation, and cell metabolism in epithelial cells [23]. Activation of LKB1 activation occurs via allosteric binding of LKB1 to STE20-related adaptor (*STRAD*) and mouse protein 25 (MO25, encoded by *CAB39* and *CAB39L*) [24]. Many of the best-known functions of LKB1 are attributable to its ability to activate AMPK, which is an important conserved regulator of cell growth and metabolism [25]. It was reported recently that activation of AMPK in myofibroblasts from IPF lungs displays lower fibrotic activity. In a bleomycin mouse model of lung fibrosis, metformin accelerates the resolution of well-established fibrosis in an AMPK-dependent manner [14]. This study supports a role for such an approach to reverse established fibrosis by facilitating deactivation and apoptosis of myofibroblasts [14]. In line with this, a recent study suggests that in patients with IPF and type 2

192 diabetes, metformin therapy may be associated with improved clinical outcomes. However,
193 further investigation with randomized clinical trials is necessary prior to metformin's broad
194 implementation in the clinical management of IPF [26].

195 Han and colleagues reported that kidney-specific deletion of *Lkb1* induces severe renal
196 fibrosis [27]. Similar to our findings, they found LKB1 (*STK11*) mRNA levels are not statistically
197 significant altered in fibrotic kidney samples. Instead, the expression of the allosteric activator
198 of LKB1, *CAB39L*, is significantly decreased in kidney fibrosis [27], raising its potential role in
199 the development of fibrotic disease. Coincidently, thymoquinone alleviates thioacetamide-
200 induced hepatic fibrosis by activating the LKB1-AMPK signaling pathway in mice [28]. Apart
201 from AMPK, LKB1 also activates a family of 12 "AMPK-related kinases", including BRSK1,
202 BRSK2, NUAK1, NUAK2, QIK, QSK, SIK, MARK1, MARK2, MARK3, MARK4 and
203 MELK [29]. It was shown earlier that LKB1 suppresses EMT-transcriptional factor Snail1 [30] and
204 ZEB1 [31] expression via MARK1/4 and miR-200a/c, respectively. In this study, we
205 demonstrated that LKB1 depletion induces Snail2 expression via autophagy inhibition-p62-
206 NFκB pathway in ATII cells, consistent with our previous reports [3, 16].

207 As a highly conserved process [32], autophagy has been associated with several human
208 diseases, including pulmonary fibrosis (see our recent review [33]). It has been reported that
209 LKB1 modulates autophagy activity via an AMPK-mTORC1 [34, 35] or AMPK-ULK1 (ATG1)
210 axis [36]. In ATII cells, upon LKB1 inhibition, autophagy activity is reduced, leading to EMT
211 via the p62-NFκB pathway (Fig. 4E). This drives local myofibroblast differentiation via
212 paracrine signalling.

213 In summary, this study provides novel insights into the role of epithelial LKB1 in pulmonary
214 fibrosis, highlighting the potential therapeutic intervention by targeting this pathway in IPF.

Materials and Methods

Cell Culture, reagents and transfections

Sources of cell lines, culture conditions and short interfering RNA (siRNA) transfections were reported earlier [3, 4, 5, 16, 18, 37, 38]. MRC5 lung fibroblasts were obtained from the European Collection of Authenticated Cell Cultures (ECACC). Fibroblasts were cultured in Dulbecco's Modified Eagle's Medium (DMEM) supplemented with 10% foetal bovine serum (FBS), 50 units/ml penicillin, 50µg/ml streptomycin, 2mM L-glutamine, 1mM sodium pyruvate, and 1x non-essential amino acids (all from Life Technologies). An alveolar type II (ATII) cell line [39] [40] [5] was cultured in DCCM-1 (Biological Industries Ltd) supplemented with 10% new-born calf serum (NBCS) (Life Technologies), 1% penicillin, 1% streptomycin, and 1% L-glutamine (all from Life Technologies). The human ATII cell line grows in continuous culture and expresses the ATII cell marker, pro-surfactant protein C (ProSP-C) [3, 5]. All cells were kept at 37 °C and 5 % CO_2. All cultures were tested and free of mycoplasma contamination. Details are provided in the Supplementary Methods.

Three-dimensional (3D) co-cultures

Aggregation of 3D co-cultures was achieved using Nanoshuttle-PL (Greiner Bio-One). Briefly, MRC5 fibroblasts at 80% confluence were treated with Nanoshuttle-PL for 24 h, before trypsinisation. Cells were then pipetted onto cell repellant 96-well plates sat on a magnetic drive and left to incubate at 37 °C and 5% CO_2 for a minimum of 3 h on the magnetic drive to enable the spheroid to form. The process was then repeated for control or LKB1-depleted ATII cells so they could then grow around the existing fibroblast spheroid. LKB1-depleted ATII

cells were generated by transfection with LKB1 (*STK11*) siRNA oligos at a final concentration of 35 nM using DharmaFECT 2 reagent (Dharmacon).

RNA *in situ* hybridization

In situ detection of *CAB39L* mRNA on formalin-fixed paraffin-embedded (FFPE) sections of lung tissue from patients with IPF or non-fibrotic control were performed using RNAscope® technology (Advanced Cell Diagnostics, Biotechne, Abingdon, UK) (n = 3 samples each group) [18]. *CAB39L* mRNA was detected by the predesigned probe. Briefly, lung tissue sections (thicknesses: 5 µm) were baked at 60 °C, deparaffinized in xylene, followed by dehydration in graded ethanol. Target retrieval, hybridization with target probe, amplification, and chromogenic detection were performed according to the manufacturer's recommendations (RNAscope 2.5 HD Assay-RED for FFPE tissues). Sections were counterstained with Gill's Hematoxylin and mounted with Vectamount prior to imaging. Assays were performed with positive (Peptidylprolyl Isomerase B, *PPIB*) and negative controls. Images were acquired using an Olympus Scanner VS110 (Olympus UK, Southend-on-Sea, UK).

Methods for RNA-seq and bioinformatics; western blot; real-time qPCR; immunofluorescence microscopy; luciferase reporter assay and statistical analysis were reported earlier [3, 4, 5, 16, 18, 37, 38], with details provided in the Supplementary Methods.

Acknowledgements

This project was supported by the UK Medical Research Council (MR/S025480/1), an UK Academy of Medical Sciences/the Wellcome Trust Springboard Award [SBF002\1038] and AAIR Charity. ZX and LY were supported by China Scholarship Council. YZ was supported by an Institute for Life Sciences PhD Studentship. JD was supported by the Francis Crick Institute which receives its core funding from Cancer Research UK (FC001070), the UK Medical Research Council (FC001070), and the Wellcome Trust (FC001070). We thank Carine Fixmer, Maria Lane, Benjamin Johnson, and the nurses of the Southampton Biomedical Research Unit for their help in the collection of human samples, supported by the Wessex Clinical Research Network and the National Institute of Health Research, UK. The authors gratefully acknowledge the Imaging and Microscopy Centre at the Biological Sciences (The University of Southampton) for their support and assistance in this work. For the purpose of open access, the authors have applied a CC-BY public copyright license to any Author Accepted Manuscript version arising from this submission.

Conflict of interest

The authors declare that they have no relevant conflict of interest.

Data Availability

All data generated or analysed during this study are included in the manuscript and supporting files. The RNA-seq data have been deposited in the Gene Expression Omnibus (GEO) database

(accession code GSE205970; the following secure token ifstmcyadrqvler has been created to allow review of this record while it remains in private status).

Figure Legend

Figure 1. Global transcriptomic changes in LKB1-depleted ATII cells.

A. Bar plot showing Gene Ontology (GO) enrichment of upregulated and downregulated differentially expressed genes (DEGs) in 3 groups: cellular component (orange), biological processes (yellow), and molecular functions (green). The top 10 enriched GO terms are arranged in $-\text{Log}_{10}(P\text{-value})$.

B. Scatter plot showing Gene Set Enrichment Analysis (GSEA). Results are ranked by the normalised enrichment score (NES). The colour and size of the dots represent false discovery rate (FDR) and gene counts, respectively.

Figure 2. LKB1 depletion in ATII cells induces EMT.

A. Gene Set Enrichment Analysis (GSEA) plot showing the enrichment of Hallmark_Epithelial-Mesenchymal Transition in LKB1-depleted ATII cells. Normalised enrichment score (NES) and false discovery rate (FDR) are indicated.

B. RNA-seq data showing relative expressions of *CDH1* (encoding E-cadherin), *VIM* (encoding Vimentin), *SNAI1* (encoding Snail1), *SNAI2* (encoding Snail2), *TWIST1*, *ZEB1* and *ZEB2* in LKB1-depleted ATII cells *vs.* control. Data are mean ± s.d.; n = 3 samples in each group. $^{**}P < 0.01$; $^{***}P < 0.001$; $^{****}P < 0.0001$ and ns: not significant.

C. Relative fold changes in mRNA levels of *CDH1* (E-cadherin), *VIM* (Vimentin), *SNAI1* (Snail1), *SNAI2* (Snail2), *TWIST1*, *ZEB1* and *ZEB2* in LKB1-depleted ATII cells *vs.* control. *ACTB* (encoding β-actin)-normalised mRNA levels in ATII cells were used to set the baseline value at unity. Data are mean ± s.d.; n = 3 samples in each group. $^{*}P < 0.05$; $^{**}P < 0.01$; $^{***}P < 0.001$ and ns: not significant.

D. Protein expressions of E-cadherin, Snail2, and LKB1 in ATII cells transfected with the indicated siRNA. β-tubulin was used as a loading control.

Figure 3. LKB1 depletion leads to autophagy inhibition-mediated EMT via the p62-NFκB-Snail2 pathway in ATII cells.

A. Protein expressions of LC3-I, LC3-II, p62 and LKB1 in ATII cells transfected with the indicated siRNA. β-actin was used as a loading control.

B. Immunofluorescence staining of p62 (red) in ATII cells transfected with the indicated siRNA. DAPI (blue) was used to stain nuclei. Scale bar: 40 μm.

C. NF-κB reporter assays in ATII cells with the indicated treatment. Values represent the relative fold of *Renilla* luciferase, normalised against control (1.0). Data are mean ± s.d.; n = 3 samples in each group. $^{**}P < 0.01$.

D. Protein expression of Snail2, p65 and LKB1 in ATII cells with the indicated treatment. β-tubulin was used as a loading control.

E. Protein expression of Snail2, p62 and LKB1 in ATII cells with the indicated treatment. β-actin was used as a loading control.

Figure 4. Down-regulation of *CAB39L* in human IPF lungs.

A. Expression of *CAB39L* in healthy (control) alveolar septae, IPF alveolar septae and IPF fibroblast foci (n = 10 individual healthy and IPF donors; GSE169500). Relative expression levels are calculated as Fragments Per Kilobase of transcript per Million mapped reads (FPKM). Data are mean ± s.d.; n = 10 samples in each group. $^{*}P < 0.05$; $^{**}P < 0.01$ and $^{***}P < 0.001$.

B. Relative fold changes in the mRNA level of *CAB39L* in human non-fibrotic control v*s.* IPF lung tissue. Data are mean ± s.d.; n = 6 samples in each group. **P* < 0.05.

C. Representative images of mRNA expression of *CAB39L* (arrows) in non-fibrotic control or IPF lung tissue using RNAscope® RNA *in-situ* hybridisation. Scale bar: 20 μm.

D. Scatter plot to compare the expression of *CAB39L* and *SNAI2* (Snail2) in alveolar septae from non-fibrotic control and IPF lung tissue. (Pearson coefficient r = - 0.65; *P* = 0.002; n = 20).

E. Diagram showing that *CAB39L* downregulation in IPF inactivates LKB1 complex, leading to autophagy inhibition-mediated EMT via the p62-NFκB-Snail2 pathway in ATII cells.

Figure 5. 3D co-cultures of ATII cells and MRC5 coupled with RNA-seq suggest a role of paracrine signalling in augmenting myofibroblast differentiation.

A. A representative image showing a 3D co-culture spheroid of MRC5 lung fibroblasts (green) and ATII cells (red). Scale bar: 250 μm.

B. Heatmap and hierarchical cluster analysis of multiple collagen genes in 2D-cultured control or LKB1-depleted ATII cells and 3D co-cultures of MRC5 with control or LKB1-depleted ATII cells. Red indicates up-regulation and blue down-regulation. n = 3 samples in each group.

C. Graph showing Gene Set Variation Analysis (GSVA) scores using a collagen signature in 2D-cultured control or LKB1-depleted ATII cells, and 3D co-cultures of MRC5 with control or LKB1-depleted ATII cells. Data are mean ± s.d.; n = 3 samples in each group. ***P* < 0.01 and ns: not significant.

D. Relative mRNA expressions of *STK11* (encoding LKB1)*, ACTA2* (encoding α-SMA), *COL1A1*, *COL3A1* and *FN1* in the spheroid samples from MRC5 co-cultured with control or

LKB1-depleted ATII cells. *ACTB* (encoding β-actin)-normalised mRNA levels in ATII cells were used to set the baseline value at unity. Data are mean ± s.d.; n = 3 samples in each group. $^{**}P < 0.01$; $^{***}P < 0.001$ and $^{****}P < 0.0001$.

E. Protein expression of α-SMA and phospho-Smad2 (p-Smad2) in MRC5 with indicated treatments. β-tubulin was used as a loading control.

References

1. Velagacherla V, Mehta CH, Nayak Y, Nayak UY. Molecular pathways and role of epigenetics in the idiopathic pulmonary fibrosis. *Life Sciences* 2022**:** 120283.

2. Raghu G, Selman M. Nintedanib and pirfenidone. New antifibrotic treatments indicated for idiopathic pulmonary fibrosis offer hopes and raises questions. American Thoracic Society; 2015. pp. 252-254.

3. Hill C, Li J, Liu D, Conforti F, Brereton CJ, Yao L*, et al.* Autophagy inhibition-mediated epithelial–mesenchymal transition augments local myofibroblast differentiation in pulmonary fibrosis. *Cell death & disease* 2019, **10**(8)**:** 1-11.

4. Yao L, Zhou Y, Li J, Wickens L, Conforti F, Rattu A*, et al.* Bidirectional epithelial–mesenchymal crosstalk provides self-sustaining profibrotic signals in pulmonary fibrosis. *Journal of Biological Chemistry* 2021, **297**(3).

5. Yao L, Conforti F, Hill C, Bell J, Drawater L, Li J*, et al.* Paracrine signalling during ZEB1-mediated epithelial–mesenchymal transition augments local myofibroblast differentiation in lung fibrosis. *Cell Death & Differentiation* 2019, **26**(5)**:** 943-957.

6. Jolly MK, Celià-Terrassa T. Dynamics of phenotypic heterogeneity associated with EMT and stemness during cancer progression. *Journal of Clinical Medicine* 2019, **8**(10)**:** 1542.

7. Hill C, Jones MG, Davies DE, Wang Y. Epithelial-mesenchymal transition contributes to pulmonary fibrosis via aberrant epithelial/fibroblastic cross-talk. *Journal of lung health and diseases* 2019, **3**(2)**:** 31.

8. Martinez-Lopez N, Athonvarangkul D, Singh R. Autophagy and aging. *Longevity Genes* 2015**:** 73-87.

9. Araya J, Kojima J, Takasaka N, Ito S, Fujii S, Hara H*, et al.* Insufficient autophagy in idiopathic pulmonary fibrosis. *American Journal of Physiology-Lung Cellular and Molecular Physiology* 2013, **304**(1)**:** L56-L69.

10. Patel AS, Lin L, Geyer A, Haspel JA, An CH, Cao J*, et al.* Autophagy in idiopathic pulmonary fibrosis. *PloS one* 2012, **7**(7)**:** e41394.

11. Wang K, Zhang T, Lei Y, Li X, Jiang J, Lan J*, et al.* Identification of ANXA2 (annexin A2) as a specific bleomycin target to induce pulmonary fibrosis by impeding TFEB-mediated autophagic flux. *Autophagy* 2018, **14**(2)**:** 269-282.

12. Ricci A, Cherubini E, Scozzi D, Pietrangeli V, Tabbì L, Raffa S*, et al.* Decreased expression of autophagic beclin 1 protein in idiopathic pulmonary fibrosis fibroblasts. *Journal of Cellular Physiology* 2013, **228**(7)**:** 1516-1524.

13. Cabrera S, Maciel M, Herrera I, Nava T, Vergara F, Gaxiola M*, et al.* Essential role for the ATG4B protease and autophagy in bleomycin-induced pulmonary fibrosis. *Autophagy* 2015, **11**(4)**:** 670-684.

14. Rangarajan S, Bone NB, Zmijewska AA, Jiang S, Park DW, Bernard K*, et al.* Metformin reverses established lung fibrosis in a bleomycin model. *Nature medicine* 2018, **24**(8)**:** 1121-1127.

15. Subramanian A, Tamayo P, Mootha VK, Mukherjee S, Ebert BL, Gillette MA*, et al.* Gene set enrichment analysis: a knowledge-based approach for interpreting genome-wide expression profiles. *Proceedings of the National Academy of Sciences* 2005, **102**(43)**:** 15545-15550.

16. Wang Y, Xiong H, Liu D, Hill C, Ertay A, Li J*, et al.* Autophagy inhibition specifically promotes epithelial-mesenchymal transition and invasion in RAS-mutated cancer cells. *Autophagy* 2019, **15**(5)**:** 886-899.

17. Zeqiraj E, Filippi BM, Deak M, Alessi DR, van Aalten DMF. Structure of the LKB1-STRAD-MO25 complex reveals an allosteric mechanism of kinase activation. *Science* 2009, **326**(5960)**:** 1707-1711.

18. Brereton CJ, Yao L, Davies ER, Zhou Y, Vukmirovic M, Bell JA*, et al.* Pseudohypoxic HIF pathway activation dysregulates collagen structure-function in human lung fibrosis. *Elife* 2022, **11:** e69348.

19. Hänzelmann S, Castelo R, Guinney J. GSVA: gene set variation analysis for microarray and RNA-Seq data. *BMC Bioinformatics* 2013, **14**(1)**:** 7.

20. Richeldi L, Collard HR, Jones MG. Idiopathic pulmonary fibrosis. *The Lancet* 2017, **389**(10082)**:** 1941-1952.

21. Moss BJ, Ryter SW, Rosas IO. Pathogenic Mechanisms Underlying Idiopathic Pulmonary Fibrosis. *Annual Review of Pathology: Mechanisms of Disease* 2022, **17**(1)**:** 515-546.

22. KING JR TE, Schwarz MI, Brown K, Tooze JA, Colby TV, Waldron Jr JA*, et al.* Idiopathic pulmonary fibrosis: relationship between histopathologic features and mortality. *American journal of respiratory and critical care medicine* 2001, **164**(6)**:** 1025-1032.

23. Kullmann L, Krahn MP. Controlling the master—upstream regulation of the tumor suppressor LKB1. *Oncogene* 2018, **37**(23)**:** 3045-3057.

24. Momcilovic M, Shackelford DB. Targeting LKB1 in cancer – exposing and exploiting vulnerabilities. *Br J Cancer* 2015, **113**(4)**:** 574-584.

25. Mihaylova MM, Shaw RJ. The AMPK signalling pathway coordinates cell growth, autophagy and metabolism. *Nature Cell Biology* 2011, **13**(9)**:** 1016-1023.

26. Teague TT, Payne SR, Kelly BT, Dempsey TM, McCoy RG, Sangaralingham LR*, et al.* Evaluation for clinical benefit of metformin in patients with idiopathic pulmonary fibrosis and type 2 diabetes mellitus: a national claims-based cohort analysis. *Respir Res* 2022, **23**(1)**:** 91.

27. Han SH, Malaga-Dieguez L, Chinga F, Kang HM, Tao J, Reidy K*, et al.* Deletion of Lkb1 in renal tubular epithelial cells leads to CKD by altering metabolism. *Journal of the American Society of Nephrology* 2016, **27**(2)**:** 439-453.

28. Bai T, Yang Y, Wu Y-L, Jiang S, Lee JJ, Lian L-H*, et al.* Thymoquinone alleviates thioacetamide-induced hepatic fibrosis and inflammation by activating LKB1–AMPK signaling pathway in mice. *International immunopharmacology* 2014, **19**(2)**:** 351-357.

29. Lizcano JM, Göransson O, Toth R, Deak M, Morrice NA, Boudeau J*, et al.* LKB1 is a master kinase that activates 13 kinases of the AMPK subfamily, including MARK/PAR-1. *The EMBO Journal* 2004, **23**(4)**:** 833-843.

30. Goodwin JM, Svensson RU, Lou HJ, Winslow MM, Turk BE, Shaw RJ. An AMPK-independent signaling pathway downstream of the LKB1 tumor suppressor controls Snail1 and metastatic potential. *Molecular cell* 2014, **55**(3)**:** 436-450.

31. Roy BC, Kohno T, Iwakawa R, Moriguchi T, Kiyono T, Morishita K*, et al.* Involvement of LKB1 in epithelial–mesenchymal transition (EMT) of human lung cancer cells. *Lung Cancer* 2010, **70**(2)**:** 136-145.

32. Hill C, Wang Y. The importance of epithelial-mesenchymal transition and autophagy in cancer drug resistance. *Cancer drug resistance (Alhambra, Calif)* 2020, **3**(1)**:** 38.

33. Hill C, Wang Y. Autophagy in Pulmonary Fibrosis: Friend or Foe? *Genes & Diseases* 2021.

34. Gurumurthy S, Xie SZ, Alagesan B, Kim J, Yusuf RZ, Saez B*, et al.* The Lkb1 metabolic sensor maintains haematopoietic stem cell survival. *Nature* 2010, **468**(7324)**:** 659-663.

35. Araya J, Nishimura SL. Fibrogenic reactions in lung disease. *Annual Review of Pathology: Mechanisms of Disease* 2010, **5:** 77-98.

36. Sanchez-Garrido J, Shenoy AR. Regulation and repurposing of nutrient sensing and autophagy in innate immunity. *Autophagy* 2021, **17**(7)**:** 1571-1591.

37. Zhou Y, Hill C, Yao L, Li J, Hancock D, Downward J*, et al.* Quantitative Proteomic Analysis in Alveolar Type II Cells Reveals the Different Capacities of RAS and TGF-β to Induce Epithelial–Mesenchymal Transition. *Frontiers in molecular biosciences* 2021, **8:** 41.

38. Wang Y, Bu F, Royer C, Serres S, Larkin JR, Soto Manuel S*, et al.* ASPP2 controls epithelial plasticity and inhibits metastasis through β-catenin-dependent regulation of ZEB1. *Nature Cell Biology* 2014, **16**(11)**:** 1092-1104.

39. Coelho MA, de Carné Trécesson S, Rana S, Zecchin D, Moore C, Molina-Arcas M*, et al.* Oncogenic RAS signaling promotes tumor immunoresistance by stabilizing PD-L1 mRNA. *Immunity* 2017, **47**(6)**:** 1083-1099. e1086.

40. Molina-Arcas M, Hancock DC, Sheridan C, Kumar MS, Downward J. Coordinate direct input of both KRAS and IGF1 receptor to activation of PI3 kinase in KRAS-mutant lung cancer. *Cancer discovery* 2013, **3**(5)**:** 548-563.

Figure 1

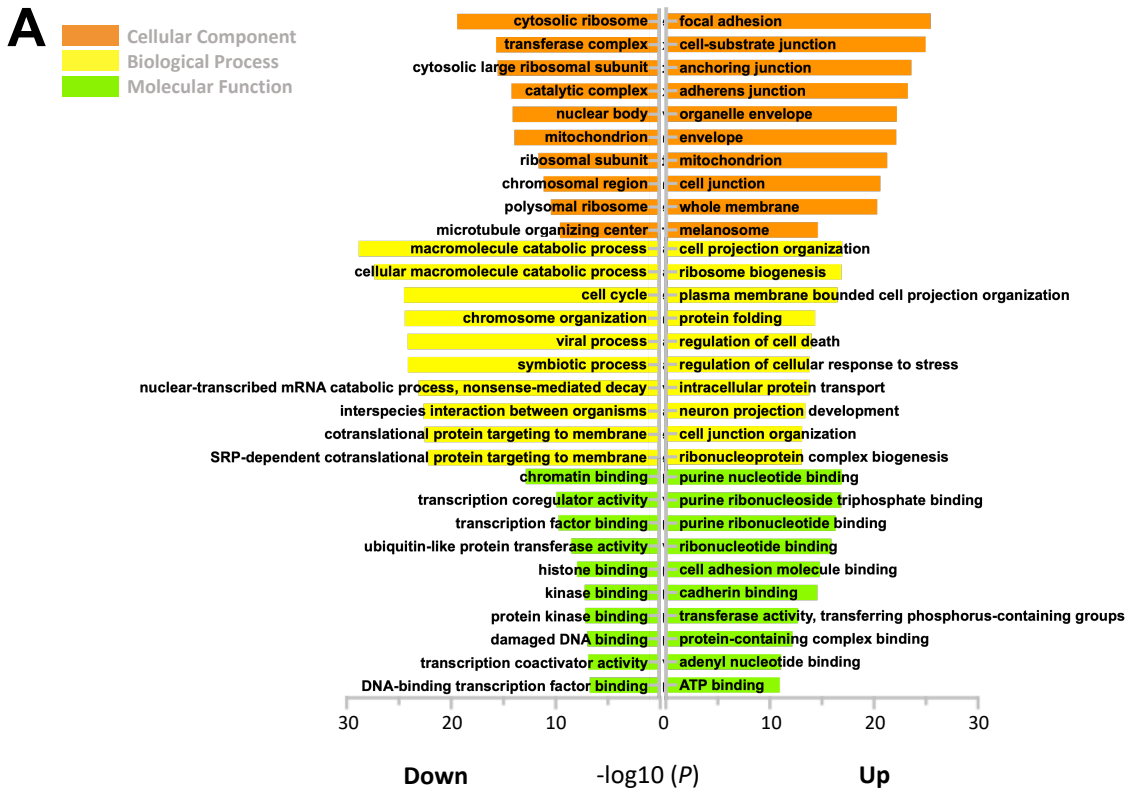
A
Cellular Component
Biological Process
Molecular Function
cytosolic ribosome
transferase complex
cytosolic large ribosomal subunit
catalytic complex
nuclear body
mitochondrion
ribosomal subunit
chromosomal region
polysomal ribosome
microtubule organizing center
macromolecule catabolic process
cellular macromolecule catabolic process
cell cycle
chromosome organization
viral process
symbiotic process
nuclear-transcribed mRNA catabolic process, nonsense-mediated decay
interspecies interaction between organisms
cotranslational protein targeting to membrane
SRP-dependent cotranslational protein targeting to membrane
chromatin binding
transcription coregulator activity
transcription factor binding
ubiquitin-like protein transferase activity
histone binding
kinase binding
protein kinase binding
damaged DNA binding
transcription coactivator activity
DNA-binding transcription factor binding
focal adhesion
cell-substrate junction
anchoring junction
adherens junction
organelle envelope
envelope
mitochondrion
cell junction
whole membrane
melanosome
cell projection organization
ribosome biogenesis
plasma membrane bounded cell projection organization
protein folding
regulation of cell death
regulation of cellular response to stress
intracellular protein transport
neuron projection development
cell junction organization
ribonucleoprotein complex biogenesis
purine nucleotide binding
purine ribonucleoside triphosphate binding
purine ribonucleotide binding
ribonucleotide binding
cell adhesion molecule binding
cadherin binding
transferase activity, transferring phosphorus-containing groups
protein-containing complex binding
adenyl nucleotide binding
ATP binding
30
20
10
0
10
20
30
Down
-log10 (P)
Up

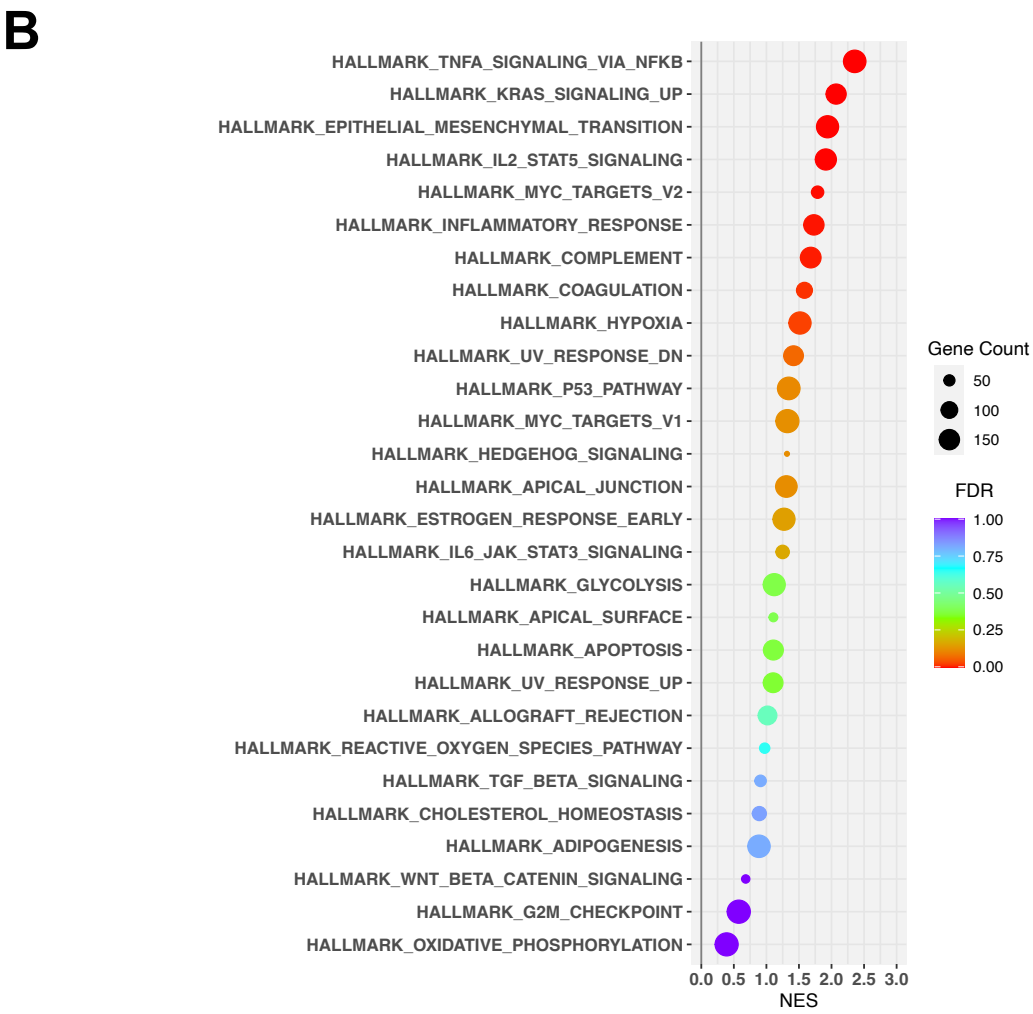
B
HALLMARK_TNFA_SIGNALING_VIA_NFKB
HALLMARK_KRAS_SIGNALING_UP
HALLMARK_EPITHELIAL_MESENCHYMAL_TRANSITION
HALLMARK_IL2_STAT5_SIGNALING
HALLMARK_MYC_TARGETS_V2
HALLMARK_INFLAMMATORY_RESPONSE
HALLMARK_COMPLEMENT
HALLMARK_COAGULATION
HALLMARK_HYPOXIA
HALLMARK_UV_RESPONSE_DN
HALLMARK_P53_PATHWAY
HALLMARK_MYC_TARGETS_V1
HALLMARK_HEDGEHOG_SIGNALING
HALLMARK_APICAL_JUNCTION
HALLMARK_ESTROGEN_RESPONSE_EARLY
HALLMARK_IL6_JAK_STAT3_SIGNALING
HALLMARK_GLYCOLYSIS
HALLMARK_APICAL_SURFACE
HALLMARK_APOPTOSIS
HALLMARK_UV_RESPONSE_UP
HALLMARK_ALLOGRAFT_REJECTION
HALLMARK_REACTIVE_OXYGEN_SPECIES_PATHWAY
HALLMARK_TGF_BETA_SIGNALING
HALLMARK_CHOLESTEROL_HOMEOSTASIS
HALLMARK_ADIPOGENESIS
HALLMARK_WNT_BETA_CATENIN_SIGNALING
HALLMARK_G2M_CHECKPOINT
HALLMARK_OXIDATIVE_PHOSPHORYLATION
0.0 0.5 1.0 1.5 2.0 2.5 3.0
NES
Gene Count
50
100
150
FDR
1.00
0.75
0.50
0.25
0.00

Figure 2

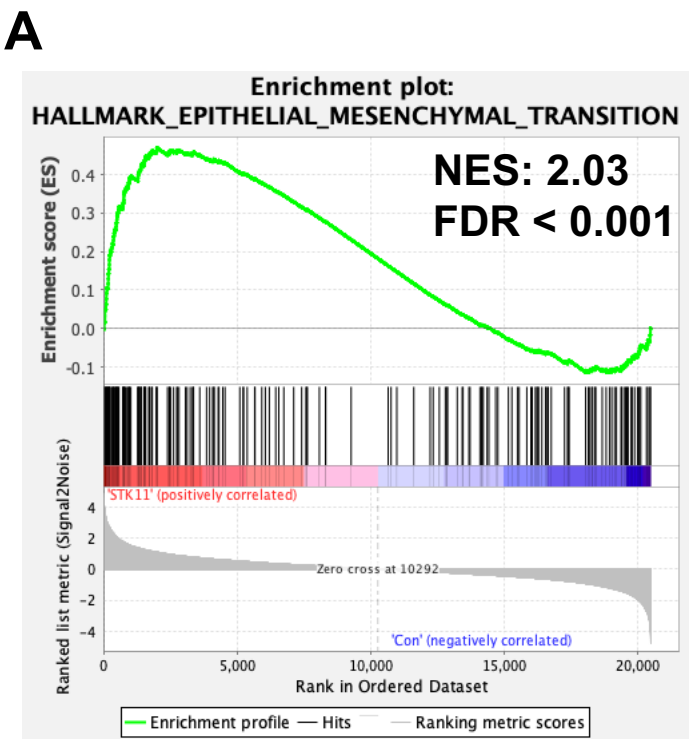
A
Enrichment plot:
HALLMARK_EPITHELIAL_MESENCHYMAL_TRANSITION
NES: 2.03
FDR < 0.001
Enrichment score (ES)
0.4
0.3
0.2
0.1
0.0
-0.1
'STK11' (positively correlated)
Ranked list metric (Signal2Noise)
4
2
0
-2
-4
Zero cross at 10292
'Con' (negatively correlated)
0
5,000
10,000
15,000
20,000
Rank in Ordered Dataset
Enrichment profile
Hits
Ranking metric scores

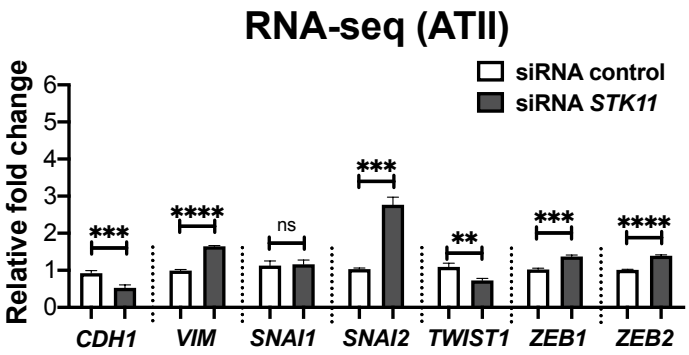
B
RNA-seq (ATII)
siRNA control
siRNA STK11
Relative fold change
6
5
4
3
2
1
0
***
****
ns
***
**
***
****
CDH1
VIM
SNAI1
SNAI2
TWIST1
ZEB1
ZEB2

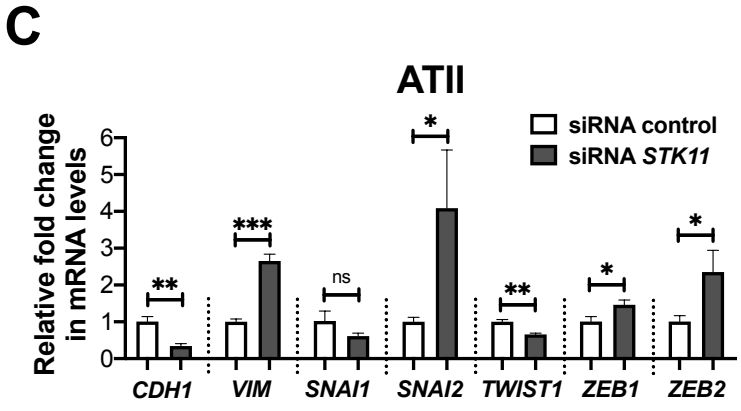
C
ATII
siRNA control
siRNA STK11
Relative fold change in mRNA levels
6
5
4
3
2
1
0
**
***
ns
*
**
*
*
CDH1
VIM
SNAI1
SNAI2
TWIST1
ZEB1
ZEB2

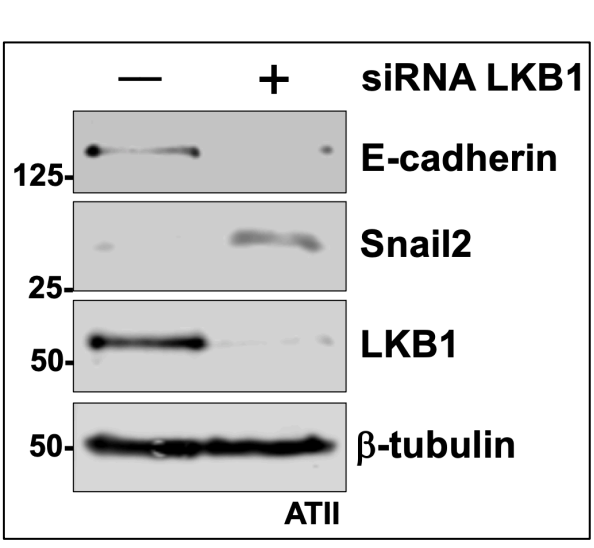
D
—
+
siRNA LKB1
125-
E-cadherin
Snail2
25-
LKB1
50-
β-tubulin
50-
ATII

Figure 3

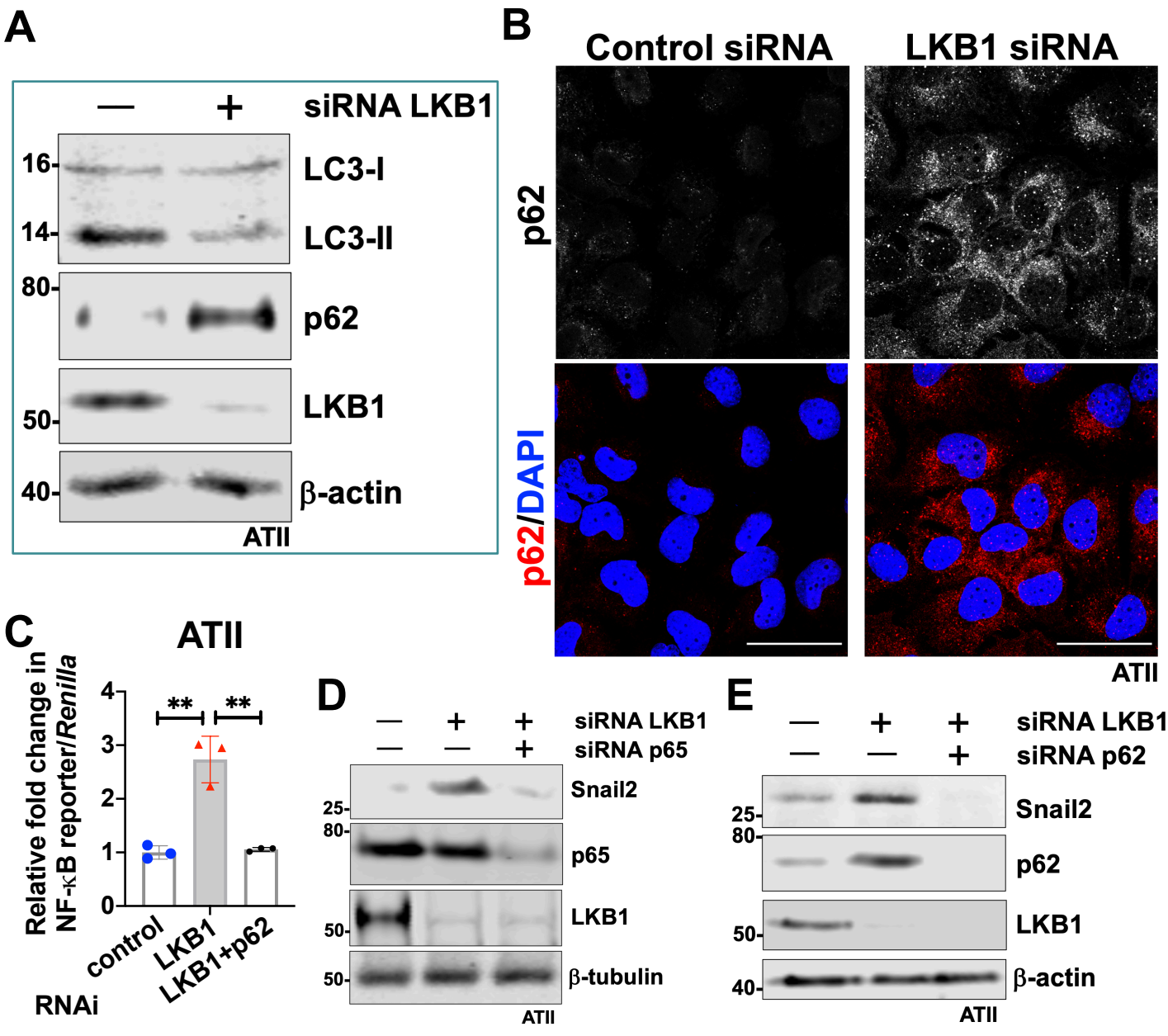
A
— + siRNA LKB1
16-
14-
80-
50-
40-
LC3-I
LC3-II
p62
LKB1
β-actin
ATII
B
Control siRNA
LKB1 siRNA
p62
p62/DAPI
ATII
C
ATII
Relative fold change in NF-κB reporter/Renilla
4
3
2
1
0
**
**
control
LKB1
LKB1+p62
RNAi
D
— + + siRNA LKB1
— — + siRNA p65
25-
80-
50-
50-
Snail2
p65
LKB1
β-tubulin
ATII
E
— + + siRNA LKB1
— — + siRNA p62
25-
80-
50-
40-
Snail2
p62
LKB1
β-actin
ATII

Figure 4

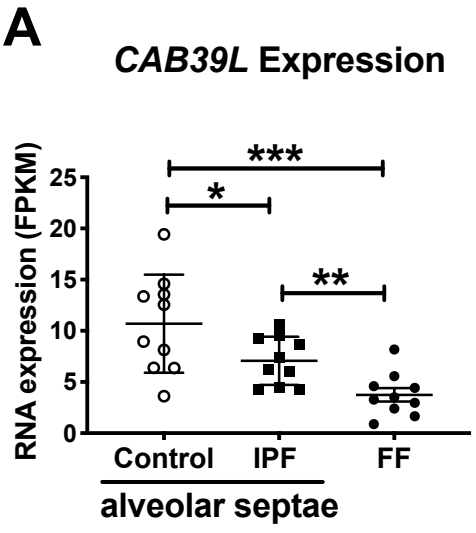
A
CAB39L Expression
RNA expression (FPKM)
25
20
15
10
5
0
***
*
**
Control
IPF
FF
alveolar septae

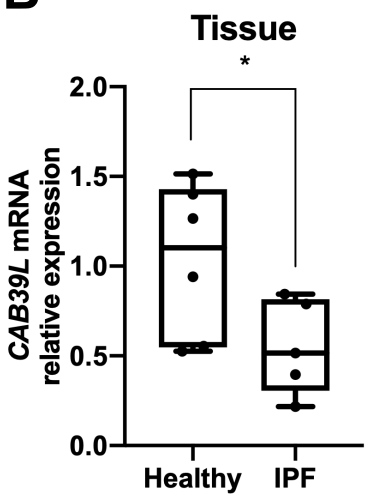
B
Tissue
*
CAB39L mRNA relative expression
2.0
1.5
1.0
0.5
0.0
Healthy
IPF

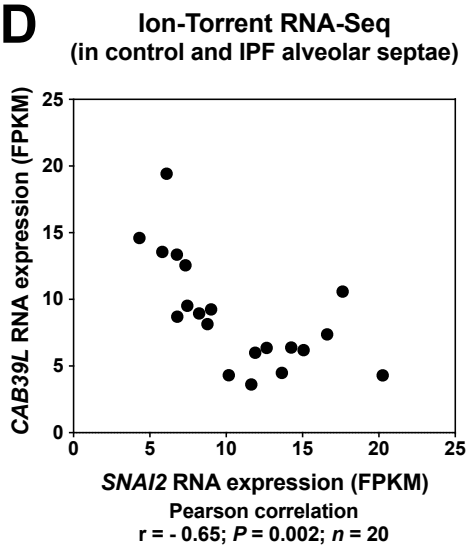
D
Ion-Torrent RNA-Seq
(in control and IPF alveolar septae)
CAB39L RNA expression (FPKM)
25
20
15
10
5
0
0
5
10
15
20
25
SNAI2 RNA expression (FPKM)
Pearson correlation
r = - 0.65; P = 0.002; n = 20

C

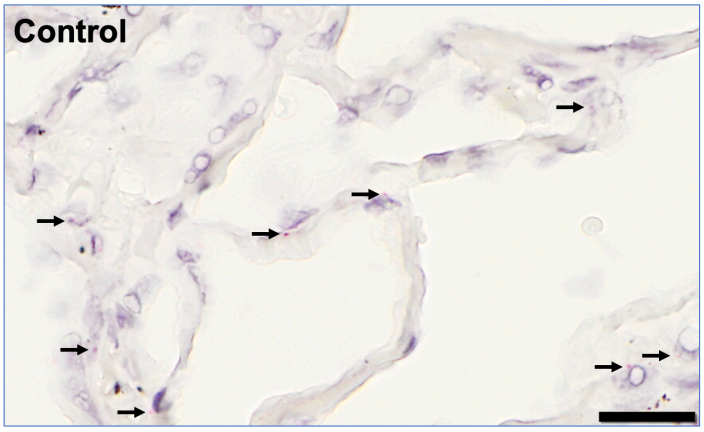
Control

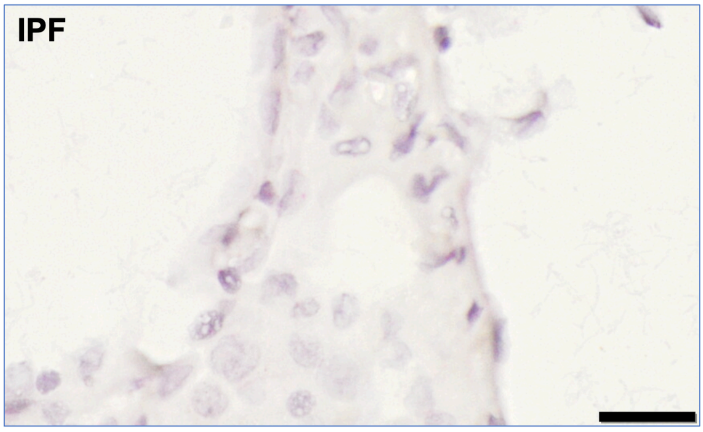
IPF

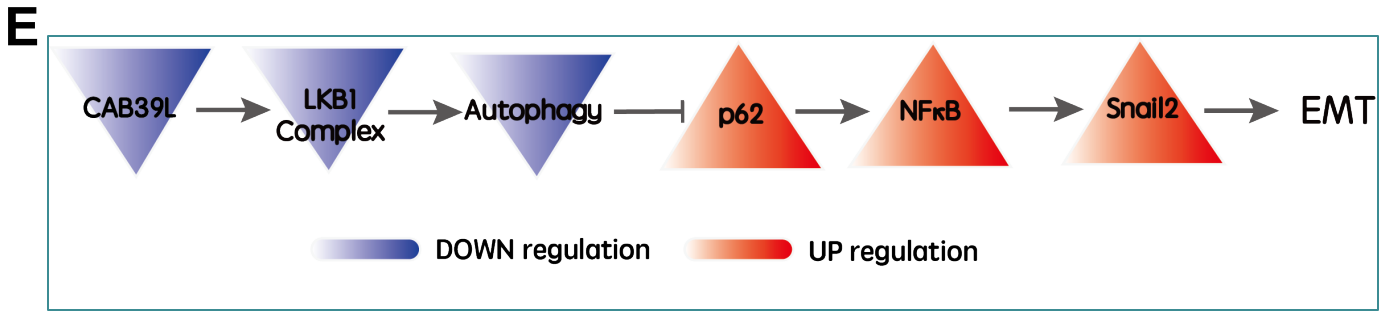
E
CAB39L
LKB1 Complex
Autophagy
p62
NFκB
Snail2
EMT
DOWN regulation
UP regulation

Figure 5

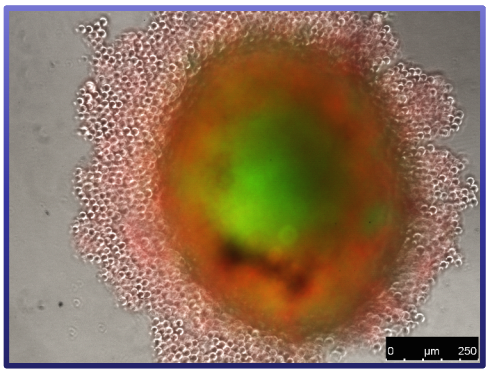
0 µm 250

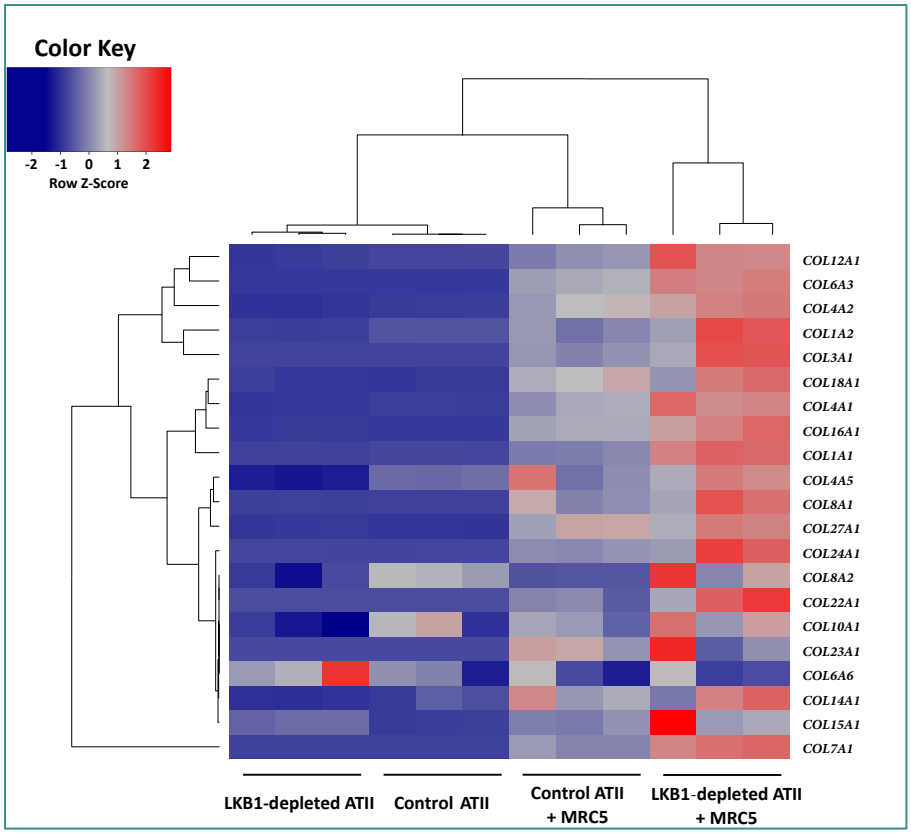
Color Key
-2 -1 0 1 2
Row Z-Score
COL12A1
COL6A3
COL4A2
COL1A2
COL3A1
COL18A1
COL4A1
COL16A1
COL1A1
COL4A5
COL8A1
COL27A1
COL24A1
COL8A2
COL22A1
COL10A1
COL23A1
COL6A6
COL14A1
COL15A1
COL7A1
LKB1-depleted ATII
Control ATII
Control ATII + MRC5
LKB1-depleted ATII + MRC5

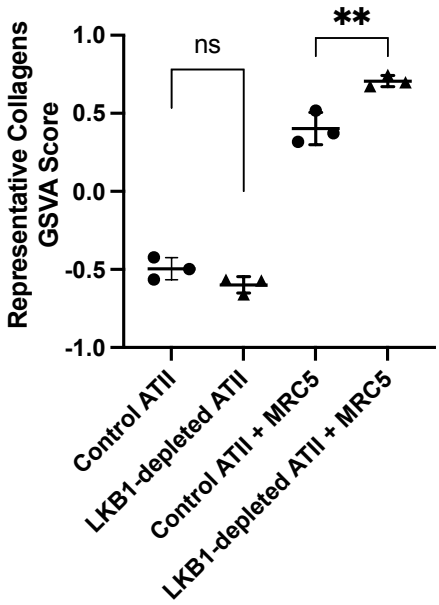
Representative Collagens GSVA Score
1.0
0.5
0.0
-0.5
-1.0
ns
**
Control ATII
LKB1-depleted ATII
Control ATII + MRC5
LKB1-depleted ATII + MRC5

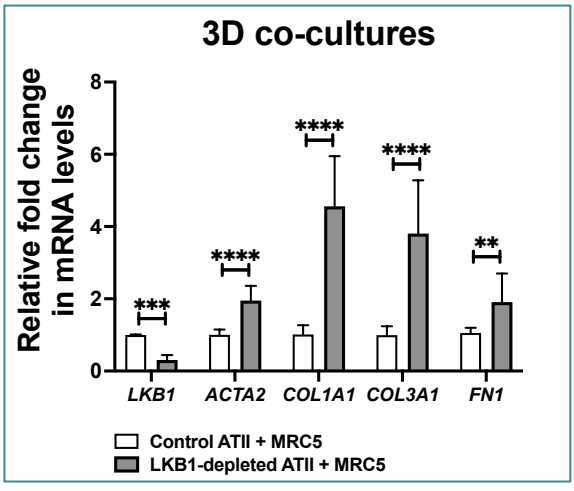
3D co-cultures
Relative fold change in mRNA levels
8
6
4
2
0
***
****
****
****
**
LKB1
ACTA2
COL1A1
COL3A1
FN1
Control ATII + MRC5
LKB1-depleted ATII + MRC5

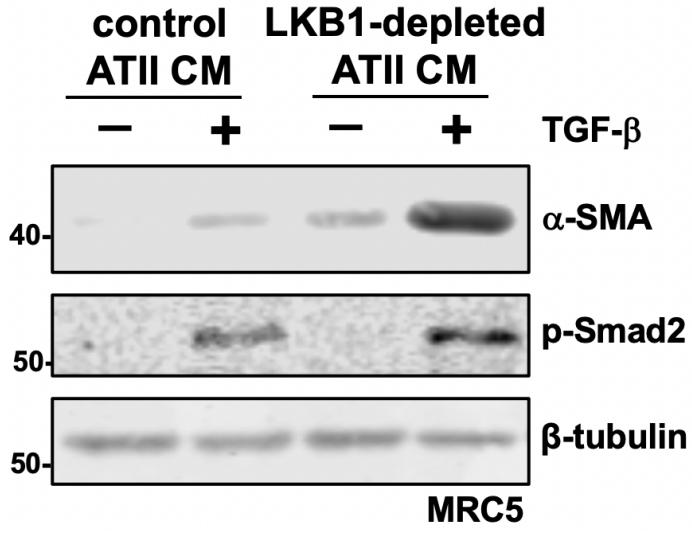
control ATII CM
LKB1-depleted ATII CM
–
+
–
+
TGF-β
40
α-SMA
50
p-Smad2
50
β-tubulin
MRC5

LKB1 inhibition in alveolar epithelial cells induces fibroblast activation in pulmonary fibrosis

Supplementary Materials

Table of contents

Supplementary Methods

1. Cell culture, reagents and transfections

MRC5 lung fibroblasts were obtained from the European Collection of Authenticated Cell Cultures (ECACC). Fibroblasts were cultured in Dulbecco's Modified Eagle's Medium (DMEM) supplemented with 10% foetal bovine serum (FBS), 50 units/ml penicillin, 50µg/ml streptomycin, 2mM L-glutamine, 1mM sodium pyruvate, and 1x non-essential amino acids (all from Life Technologies). Alveolar type II (ATII) cells [1] [2] [3] were cultured in DCCM-1 (Biological Industries Ltd) supplemented with 10% new-born calf serum (NBCS) (Life Technologies), 1% penicillin, 1% streptomycin, and 1% L-glutamine (all from Life Technologies). All cells were kept at 37 °C and 5 % CO_2. All cultures were tested and free of mycoplasma contamination.

Short interfering RNA (siRNA) against *STK11* (LKB1) (M-005035-02-0010), *SQSTM1* (p62) (MU-010230-00-0002) and *RELA* (p65) (MU-003533-02-0002) were purchased from Dharmacon. Sequence is available from Dharmacon, or on request. ATII cells were transfected with the indicated siRNA at a final concentration of 35 nM using DharmaFECT 2 reagent (Dharmacon). siGENOME RISC-Free siRNA (Dharmacon) was used as a negative control.

2. Lung tissue sampling

All human lung tissue samples for primary cell culture were approved by the Southampton and South West Hampshire and the Mid and South Buckinghamshire Local Research Ethics Committees, and all subjects gave written informed consent. Clinically indicated IPF lung biopsy tissue samples and non-fibrotic control tissue samples (macroscopically normal lung sampled remote from a cancer site) were assessed as surplus to clinical diagnostic requirements. All IPF samples were from patients subsequently receiving a multidisciplinary diagnosis of IPF according to international consensus guidelines [4]

3. RNA-seq and bioinformatic analysis

RNA isolation and mRNA sequencing of samples were performed following the manufacturer's instructions (Novogene, UK). The ATII cells were treated transfected with siRNA against indicated siRNAs for 48h. Total RNA was isolated using RNeasy mini kit (Qiagen) according to manufacturer's instructions and quantified using a Nanodrop Spectophotometer 2000c (Thermo Fisher Scientific).

A total amount of 3 μg RNA per sample was used as input material for library construction. Sequencing libraries were generated using NEBNext® UltraTM RNA Library Prep Kit for Illumina® (NEB, Ipswich, Massachusetts, USA) following manufacturer's instruction. Libraries were pooled in equimolar and sequenced using the paired-end strategy (2 × 150) on the Illumina NovaSeq 6000 platform following the standard protocols (Novogene, UK). Raw read counts were imported into RStudio (version 4.2.0) and analyzed by using DESeq2 [5] (version 1.26.0). Transcripts with low abundance (under 10 counts across all samples) were removed. The R codes were provided in the Supplementary Materials. Genes with a false discovery rate (FDR) adjusted *P* value using Benjamini-Hochberg (BH) method less than 0.05 and $|Log_2FoldChange|$ above 1 were considered as differentially expressed genes (DEGs). DEGs in 2D-cultured LKB1-depleted ATII cells are provided in Table S1 and DEGs in 3D co-cultures of LKB1-depleted ATII cells and MRC5 in Table S4.

The collection of Hallmark gene sets generated from the gene set enrichment analysis (GSEA) software (version 4.1.0) (with registration) [6]. Gene Ontology (GO) terms and Hallmark enrichment analysis of DEGs were generated through DAVID website tools (https://david.ncifcrf.gov) with default parameters. FDR adjusted *P* values by Benjamini-Hochberg (BH) method were used to estimate the statistical significance. Details for GO enrichment analysis are provided in Table S2 and Gene Set Enrichment Analysis (GSEA) in Table S3.

A collagen gene score for each sample was calculated using Gene Set Variation Analysis (GSVA) based on a list of 21 collagen genes upregulated in 3D co-cultured LKB1-depleted ATII cells and MRC5 (Table S5).

4. Western blot analysis

Western blot analysis was performed with lysates from cells with Urea buffer (8 M Urea, 1 M Thiourea, 0.5% CHAPS, 50 mM DTT, and 24 mM Spermine). Primary antibodies were from: Santa Cruz (β-actin, sc-47778; Snail2, sc-10436), Abcam (β-tubulin, ab6046) and Cell Signalling Technology (α-SMA, 14968; Snail2, 9585; β-tubulin, 86298; LC3, 2775; p62/*SQSTM1*, 5114; p65/RELA, 8242; Phospho-Smad2, 3104). Signals were detected using Odyssey imaging system (LI-COR), and evaluated by ImageJ 1.42q software (National Institutes of Health).

5. Real-time qPCR analysis

Total RNA was extracted using RNeasy mini kit (Qiagen) following manufacturer's instructions. RNA concentration was quantified on a Nanodrop Spectophotometer 2000c (ThermoFisher Scientific, UK). Real-time PCR was carried out using gene-specific primers *SNAI1* (Snail1) (QT00010010), *SNAI2* (Snail2) (QT00044128), *ZEB1* (QT00008555), *ZEB2* (QT00008554), *TWIST1* (QT00011956), *STK11* (LKB1) (QT01008980), *ACTA2* (Alpha smooth muscle actin, α-SMA) (QT00088102), *COL1A1* (QT00037793), *COL3A1* (QT00058233) and *FN1* (QT00038024) or *ACTB* (β-actin) (QT01680476), QuantiNova SYBR Green RT-PCR kits (Qiagen) and QuantiTect Primer Assays(Qiagen) according to manufacturer's instruction or RNA was reverse transcribed and run with primers and Taqman probe sets obtained from Thermofisher Scientific, Reading UK. Relative transcript levels of target genes were normalised to *ACTB* (β-actin).

6. Immunofluorescence microscopy

The immunofluorescence assay was performed as previously described [7]. When the cells reached 80 - 90% confluency, media were removed and cells were gently washed with 1× PBS twice. One ml 4% paraformaldehyde (PFA) (Thermo Fisher Scientific, UK) in 1× PBS was added to fix the cells for 15 minutes. PFA was then removed and cells were washed with 1× PBS. For permeabilisation of cells, 500 µl of 0.1% TironX-100 (Thermo Fisher Scientific, UK) in 1× PBS was added to the each well of 12 well

plate and the slide was transferred from 6 well plate into 12 well plate and incubated in 0.1% TironX-100 for 5 minutes on ice. This was followed by washing the slides with 1× PBS twice. Then, cells on the slides were blocked in 0.2% Fish Skin Gelatine (Sigma Aldrich, UK) in 1× PBS for 60 minutes at room temperature. Meanwhile, anti-p62 primary antibody was prepared in blocking buffer with 1:50 dilution and paraflim was put on the foil wrapped container. To moisture the container, wet tissues were put into the side of box. Primary antibody was put on the paraflim and the excess buffer was got rid of from the slides and slides were put on the antibody upside down for 60 minutes at room temperature. 60 minutes after the primary antibody incubation (anti-p62/SQSTM1; Progen Biotechnik GmbH, GP62-C; 1:300), slides were flipped and put into 12 well plate and washed with 1× PBS 3 times, each time for 15 minutes on the rocker. Then, secondary antibody with 4'6-Diamidino-2-Pheylindole (DAPI) (Invitrogen, UK) was prepared in 1× PBS with the dilution of 1:400 and 1:1000, respectively. New paraflim was put into the box, 95 µl of secondary antibody was put onto paraflim, and slides were put onto paraflim upside down and incubated at room temperature for 60 minutes. Slides were washed with 1× PBS as previously by avoiding light. 8 µl of mounting solution was added to the cover slip and slide was put on the cover slip upside down and left to air dry overnight by avoiding light. Protein expression was detected using Alexa Fluor (1:400, Molecular Probes) for 20 minutes. Immunostained cells were analyzed and photographed using an Olympus IX83 inverted fluorescence microscope.

7. Luciferase reporter assay

The luciferase reporter assay was performed as previously described [3]. Cells were transfected using Lipofectamine 3000 (Life technology) in a 96-well plate with 100 ng of *Renilla* along with 100 ng of NFkB reporter per well. Cells were washed with 1 × PBS and lysed by trypsin (0.05% trypsin, Gibco), then centrifuged at 500 g for 5 minutes. Cell pellet was then re-suspended in certain amount of complete media before plating on a 96-well plate (Usually 100 µl of medium for each well) at 70-80% confluency. For each well to be transfected, 0.1 µl of Lipofectamine 3000 reagent (Life

technology) was diluted in 5 µl of Opti-MEM medium. Mixed well reagent was made and short vortexed. Diluted plasmids and Lipofectamine 3000 were mixed by pipetting up and down and the lipid-DNA mixture was incubated at room temperature for 15 minutes. Cells were transfected at 37°C for 48 hours before analysis. The transcriptional assay was carried out using the Dual-Luciferase reporter assay system (Promega, UK) following the manufacturer's protocol. Cells were wash with 1 × PBS prior to lysis in a 96-well plate. Cells were lysed in 100 µl of passive lysis buffer and put on a room temperature shaker for 15 minutes. Freezing lysates at -20 °C facilitated the lysis. Five µl of lysate was analyzed for each well in a 96 well white plate. Triplets were used for each transfection and 25 µl LAR II was first added and mixed by pipetting to measure the firefly luciferase activity. Another 25 µl of stop and go reagent was then added to help identify the *Renilla* activity. The final Dual-Luciferase Reporter activity was normalized based on both measurements.

8. Statistical analysis

Statistical analyses were performed in GraphPad Prism v7.02 (GraphPad Software Inc, San Diego, CA) unless otherwise indicated. No data were excluded from the studies and for all experiments, all attempts at replication were successful. For each experiment, sample size reflects the number of independent biological replicates and is provided in the figure legend. Normality of distribution was assessed using the D'Agostino-Pearson normality test. Statistical analyses of single comparisons of two groups utilised Student's *t*-test or Mann-Whitney *U*-test for parametric and non-parametric data respectively. Where appropriate, individual t-test results were corrected for multiple comparisons using the Holm-Sidak method. For multiple comparisons, one-way or two-way analysis of variance (ANOVA) with Dunnett's multiple comparison test or Kruskal-Wallis analysis with Dunn's multiple comparison test were used for parametric and non-parametric data, respectively. Results were considered significant if $P < 0.05$, where $*P < 0.05$, $**P < 0.01$, $***P < 0.001$, $****P < 0.0001$.

Supplementary Figures

Supplementary Figure 1. Global transcriptomic changes in LKB1-depleted ATII cells.

A. REVIGO TreeMap showing Gene Ontology (GO) analysis of upregulated differentially expressed genes (DEGs) in LKB1-depleted ATII cells. Common colours represent groupings based on parent GO terms, and each rectangle is a percentage of the relative enrichment of the GO term compared with the whole genome. Genes with a false discovery rate (FDR) less than 0.05 and $|Log_2FoldChange|$ above 1 were considered as DEGs.

B. Scatter plot showing top ten GO terms enriched by upregulated DEGs in 3 functional groups: cellular component, biological processes and molecular functions. Rich factor is the percentage of DEG-enriched gene count in the given annotated GO terms. The sizes of circles represent gene counts, and the colours of circles represent FDR.

Supplementary Figure 2. LKB1 depletion leads to autophagy inhibition-mediated EMT via the p62-NFκB-Snail2 pathway in ATII cells.

A. Gene set enrichment analysis (GSEA) plot showing an enrichment of Hallmark_TNFA_Signaling_Via_NFKB in LKB1-depleted ATII cells. Normalised enrichment score (NES) and false discovery rate (FDR) are indicated.
B. NF-κB reporter assays in ATII cells transfected with the indicated siRNA. Values represent the relative fold of firefly luciferase in relation to Renilla luciferase, normalised against control (1.0). Data are mean ± s.d.; n = 3 samples in each group. $^{**}P < 0.01$.

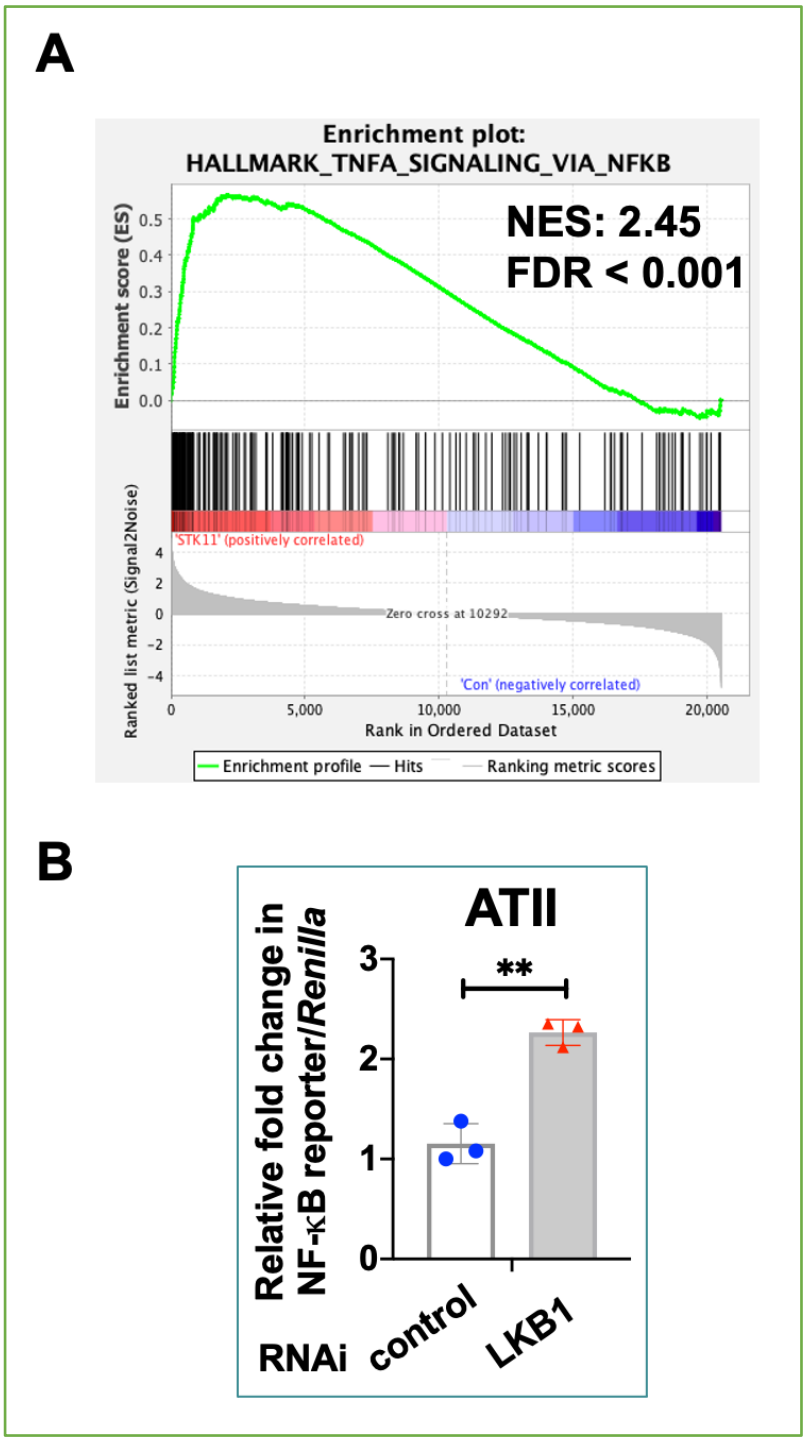

Supplementary Figure 3. **Down-regulation of *CAB39L* in human IPF lungs.** Expression of *STK11* (LKB1) (**A**), *STRADA* (**B**), *STRADB* (**C**) and *CAB39* (**D**) in healthy (control) alveolar septae, IPF alveolar septae and IPF fibroblast foci (n = 10 individual healthy and IPF donors; GSE169500). Relative expression levels are calculated as Fragments Per Kilobase of transcript per Million mapped reads (FPKM). Data are mean ± s.d.; n = 10 samples in each group.

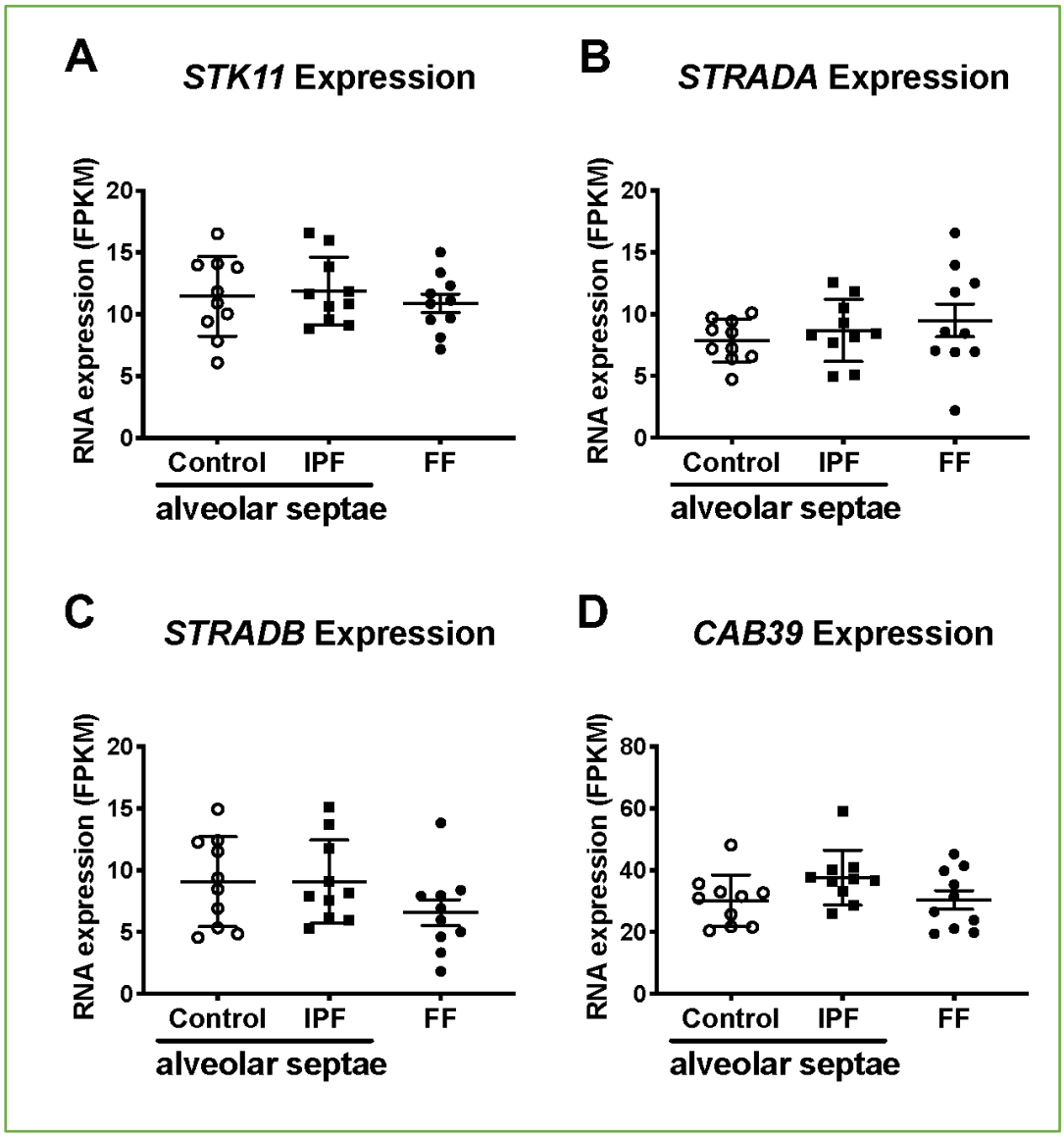

Supplementary Figure 4. 3D co-cultures of ATII cells and MRC5 coupled with RNA-seq suggest a role of paracrine signalling in augmenting myofibroblast differentiation.

A. Cell deconvolution based on an epithelial or a mesenchymal cell signature matrix derived from the single-cell RNA-seq (GSE135893) was used to determine cell compositions in spheroid samples from MRC5 co-cultured with control or LKB1-depleted ATII cells. Data are mean ± s.d.; n = 3 samples in each group. **P* < 0.05.

B. RNA-seq data showing relative expressions of *ACTA2*, *COL1A1*, *COL3A1* and *FN1* in spheroid samples from MRC5 co-cultured with control or LKB1-depleted ATII cells. Data are mean ± s.d.; n = 3 samples per group. *****P* < 0.0001 and ns: not significant.

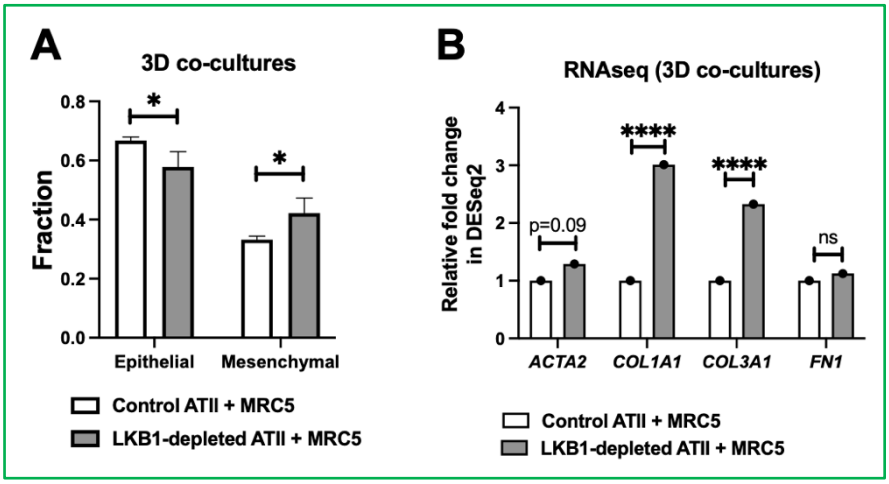

Supplementary Tables

Table S1. DEGs in LKB1-depleted alveolar type II (ATII) cells.

Table S2. GO terms enrichment analysis in LKB1-depleted ATII cells.

Table S3. GSEA in LKB1-depleted ATII cells.

Table S4. DEGs in 3D co-cultured LKB1-depleted ATII cells and MRC5.

Table S5. List of collagen genes used for GSVA calculation in Figure 5C.

R Scripts

Raw data were imported into RStudio (version 4.2.0). RStudio Version 1.4.1717 for IOS and R scripts were run.

Set the working directory before run

setwd("C:/Users/zx2n18/RNA-seq")

R codes for Figure 1B

```
library(ggplot2)
data <- read.csv ("Hallmark_gsea_Up.csv")
p <- ggplot(data, aes(NES, NAME))
p + geom_point(aes(colour=FDR.q.val, size=SIZE)) +
   scale_color_gradientn(colours=rainbow(4), limits=c(0, 1)) +
   geom_vline(xintercept=0, size=0.5, colour="gray50") +
   theme(axis.text = element_text(size = 8, face = "bold"),
panel.background=element_rect(fill="gray95", colour="gray95"),
            panel.grid.major=element_line(size=0.45,linetype='solid',
colour="gray90"),
            panel.grid.minor=element_line(size=0.45,linetype='solid',
colour="gray90"),
            axis.title.y=element_blank()) +
   expand_limits(x=c(0,3)) +
   scale_x_continuous(breaks=c(0,0.5,1,1.5,2,2.5,3)) +
   scale_y_discrete(limits=rev(data$NAME))
```

R codes for Figure 5B, S4A

```
#signature matrix building (scRNAseq by GSE13589)
library(dplyr)
source("https://z.umn.edu/archived-seurat")
library(Seurat)
library(patchwork)
install.packages('umap')
library(umap)
library(reticulate)
getwd()
setwd('/Users/lianyuanyuan/Desktop/Cell death and diease')
# Load the PBMC dataset
# Load the dataset
cell_type<-read.csv('/Users/lianyuanyuan/Library/Mobile
Documents/com~apple~CloudDocs/R/GSE135893_PF_subtypes/Control_Celltype.cs
v',header = T,sep = ',')
ppulmonary_fibrosis <- Read10X(data.dir = "/Users/lianyuanyuan/Library/Mobile
Documents/com~apple~CloudDocs/R/GSE135893_PF_subtypes/GSE135893_PF_su
btypes",gene.column = 1) ppulmonary_fibrosis_seurat <-
CreateSeuratObject(ppulmonary_fibrosis, project = "scRNA lung",min.features =
200) sc_data<-GetAssayData(object = pbmc.data, slot = 'counts')
sc_epi_mesenchymal<-sc_data[,cell_type$X]
#notice to delete the row.name with "march"or"sep" in the csv file, because that will
cause the "duplicate row.name" when you
#run it in the cibersorts.
write.table(sc_epi_mesenchymal,file='sc_epi_mesenchymal_Control_M.txt',sep =
'\t',row.names = T)
write.table(cell_type$population,file='sc_epi_mesenchymal_control_M_population.tx
t',sep = '\t',row.names = T)
```

R codes for Figure 5C

```
BiocManager::install("GSVA")
library("GSVA")
data <-read.csv("2d_3d_exprMatrix.rpm2.csv")
rownames(data)<-data[,1]
data<-data[,-1]
data<-as.matrix(data)
geneset<-read.csv("col_up_3d.csv")
GSVA <- gsva(data, geneSets, mx.diff=1)
```

R codes for Figure S1A

```
library(treemap)
revigo.names <-
c("term_ID","description","frequency","value","uniqueness","dispensability","represe
ntative");
revigo.data <- read.csv("GO_data.csv")
stuff <- data.frame(revigo.data);
names(stuff) <- revigo.names;
stuff$value <- as.numeric( as.character(stuff$value) );
stuff$frequency <- as.numeric( as.character(stuff$frequency) );
stuff$uniqueness <- as.numeric( as.character(stuff$uniqueness) );
stuff$dispensability <- as.numeric( as.character(stuff$dispensability) );
# by default, outputs to a PDF file
pdf( file="revigo_treemap.pdf", width=16, height=9 ) # width and height are in inches
# check the tmPlot command documentation for all possible parameters - there are a
lot more
treemap(
   stuff,
   index = c("representative","description"),
   vSize = "value",
   type = "categorical",
   vColor = "representative",
   title = "Revigo TreeMap",
   inflate.labels = FALSE,           # set this to TRUE for space-filling group labels -
good for posters
   lowerbound.cex.labels = 0,      # try to draw as many labels as possible (still, some
small squares may not get a label)
   bg.labels = "#CCCCCCAA",      # define background color of group labels
                                       # "#CCCCCC00" is fully transparent,
"#CCCCCCAA" is semi-transparent grey, NA is opaque
   position.legend = "none"
)
dev.off()
```

R codes for Figure S1B

```
mytheme <- theme(axis.title=element_text(face="bold", size=10,colour = 'gray25'),
axis.text=element_text(face="bold", size=10,colour = 'gray25'), axis.line =
element_line(size=0.5, colour = 'black'), panel.background =
element_rect(color='black'), legend.key = element_blank()
)
Go_Up<read.xlsx('/Toppgene_2dup_result.xlsx',sheet = 1)
Go_Up$Count<-sapply(Go_Up$InTerm_InList,function(x)
strsplit(x,"/")[[1]][1]) %>%as.numeric()
Go_Up$Member<-sapply(Go_Up$InTerm_InList,function(x)
strsplit(x,"/")[[1]][2])%>%as.numeric()
Go_Up$GeneRatio<-as.numeric(Go_Up[,10])/as.numeric(Go_Up[,11] )
Go_Up<-Go_Up[grepl('Member',Go_Up$GroupID),]
Go_Up$`P.adjust`<-10^(Go_Up$`Log(q-value)`)
Go_Up<-Go_Up[order(Go_Up$GeneRatio),]
Go_Up$Description<-factor(Go_Up$Description,levels = (Go_Up$Description))
#Plot
p<-ggplot(Go_Up,aes(GeneRatio,Description)) +

geom_point(aes(size=Count,color=`P.adjust`))+scale_colour_gradient(high='blue',low
='red',n.breaks=10)+
   theme_bw()+
   theme(axis.title=element_text(face="bold", size=10,colour = 'black'),
            axis.text=element_text(face="bold", size=10,colour = 'black'))
p
ggsave('Up_Go_result.pdf',width = 9,height = 8)
```

R codes for Figure S4B

```
library(gplots)
a1<-read.csv("colleagen_up.csv")
a1<-as.matrix(a1)
a1<-as.numeric(a1)
distCor <- function(a1) as.dist(1-cor(t(a1)))
hclustAvg <- function(a1) hclust(a1, method="average")
pdf("collagen_heatmap.pdf",width=20, height=20)# units="in", width=12, height=8,
res=300)
colorbar<-colorRampPalette(c('darkblue','grey','red'))(n=1000)
###set the color for heatmap
heatmap.2(a1, trace="none", density='none',margin=c(5,10),scale="row",cexRow =
1.3,
            #labRow = labels,
            cexCol = 0.8, zlim=c(-10,10),Colv = T,Rowv =
T,srtCol=45,adjCol=c(1,0),
            hclustfun = hclustAvg,distfun=distCor,symbreak=FALSE,key =
T,keysize = 1.5,
            #labRow =c(as.character(DEP_ras_expression_fc_pvalue$P.Value..)),

            #ColSideColors = condition_colors
            #RowSideColors=row_annotation)
)
dev.off()
```

References

1. Coelho, M.A., et al., *Oncogenic RAS signaling promotes tumor immunoresistance by stabilizing PD-L1 mRNA.* Immunity, 2017. **47**(6): p. 1083-1099. e6.
2. Molina-Arcas, M., et al., *Coordinate direct input of both KRAS and IGF1 receptor to activation of PI3 kinase in KRAS-mutant lung cancer.* Cancer discovery, 2013. **3**(5): p. 548-563.
3. Yao, L., et al., *Paracrine signalling during ZEB1-mediated epithelial–mesenchymal transition augments local myofibroblast differentiation in lung fibrosis.* Cell Death & Differentiation, 2019. **26**(5): p. 943-957.
4. Raghu, G., et al., *Diagnosis of idiopathic pulmonary fibrosis. An official ATS/ERS/JRS/ALAT clinical practice guideline.* American journal of respiratory and critical care medicine, 2018. **198**(5): p. e44-e68.
5. Love, M.I., W. Huber, and S. Anders, *Moderated estimation of fold change and dispersion for RNA-seq data with DESeq2.* Genome biology, 2014. **15**(12): p. 1-21.
6. Subramanian, A., et al., *Gene set enrichment analysis: a knowledge-based approach for interpreting genome-wide expression profiles.* Proceedings of the National Academy of Sciences, 2005. **102**(43): p. 15545-15550.
7. Ertay, A., et al., *WDHD1 is essential for the survival of PTEN-inactive triple-negative breast cancer.* Cell Death & Disease, 2020. **11**(11): p. 1001.

Raw data for western blots

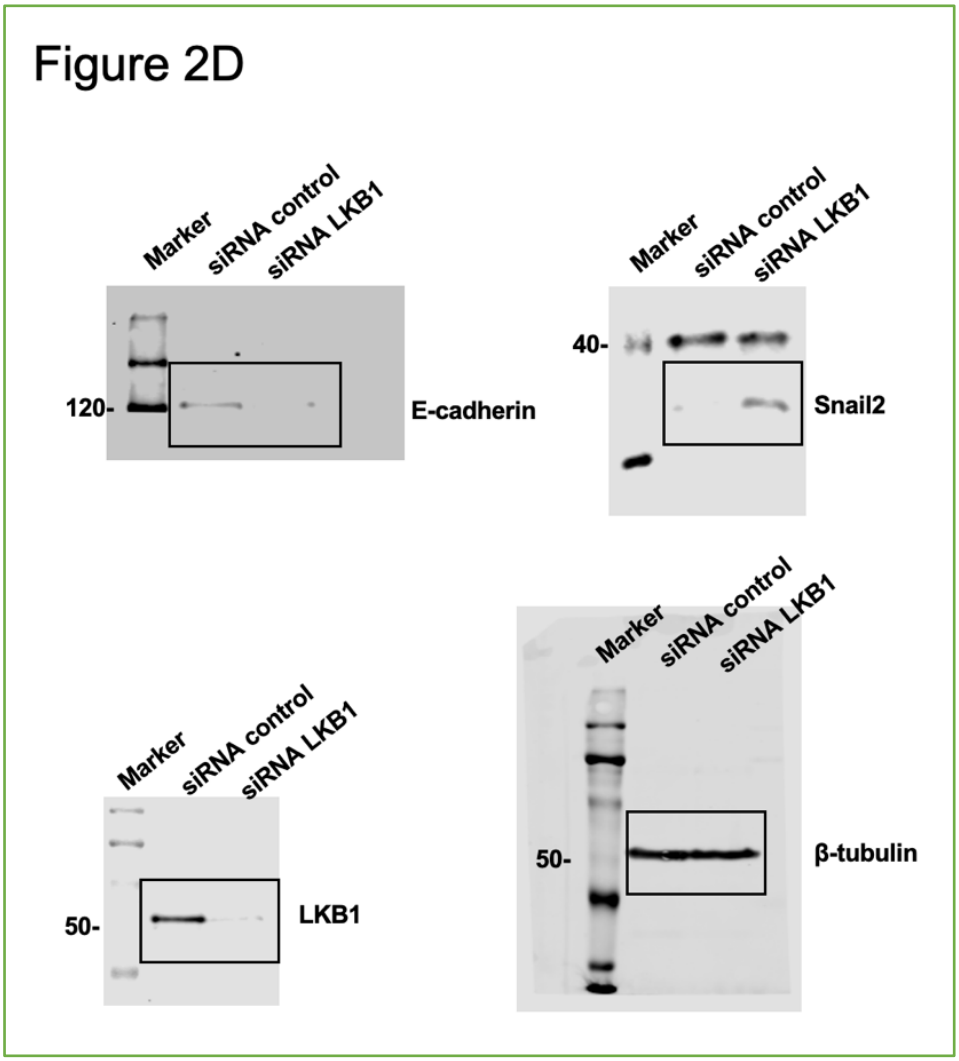

Figure 3A

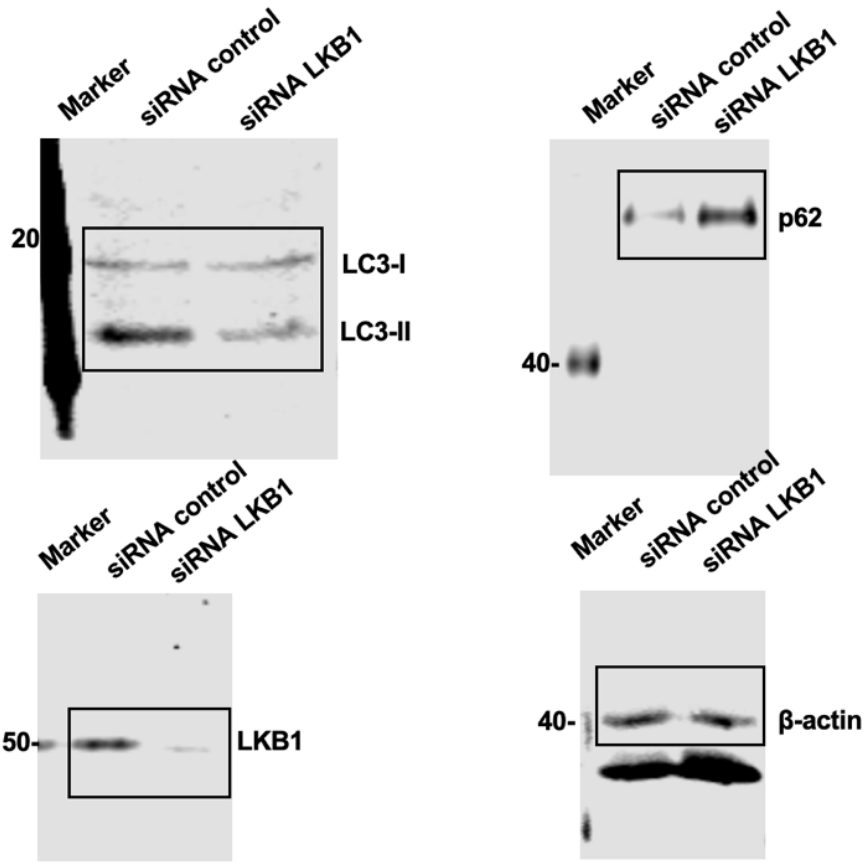
Marker
siRNA control
siRNA LKB1
20
LC3-I
LC3-II
Marker
siRNA control
siRNA LKB1
p62
40-
Marker
siRNA control
siRNA LKB1
50-
LKB1
Marker
siRNA control
siRNA LKB1
40-
β-actin

Figure 3D

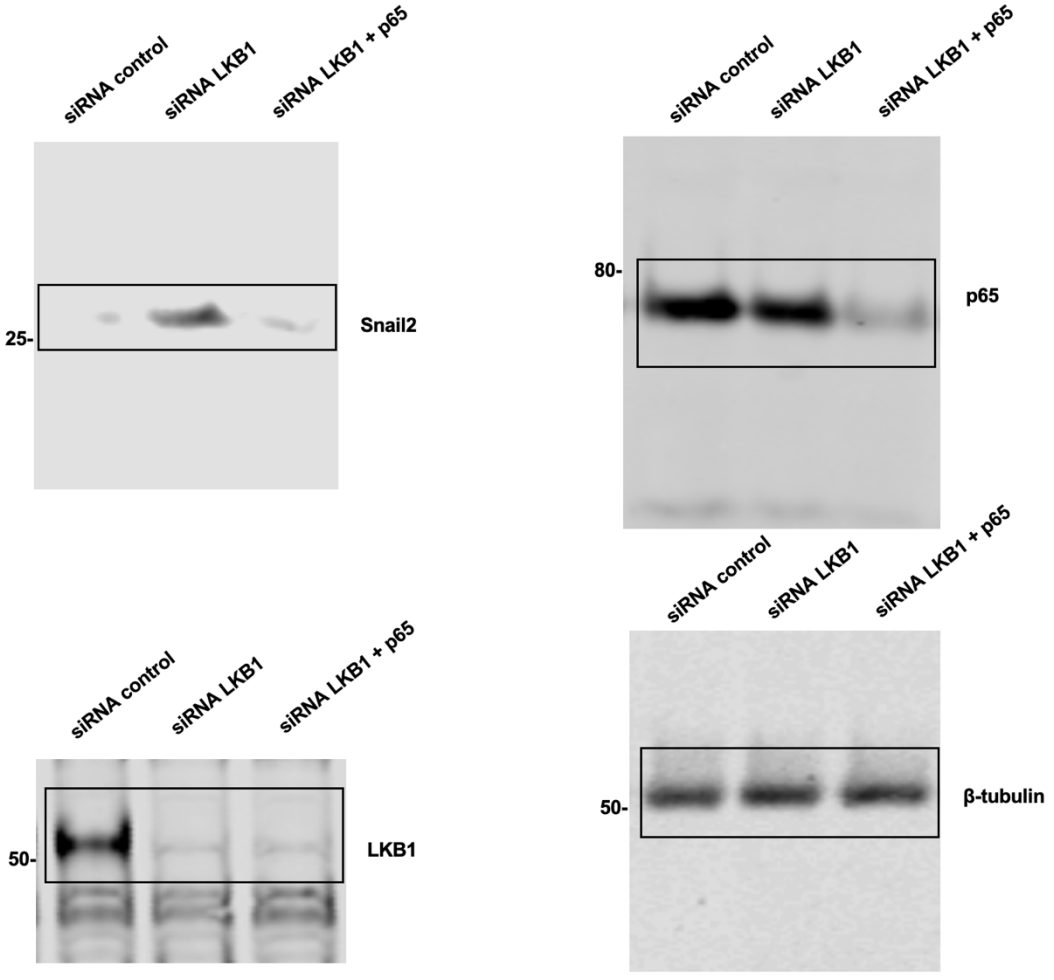
siRNA control
siRNA LKB1
siRNA LKB1 + p65
25-
Snail2
siRNA control
siRNA LKB1
siRNA LKB1 + p65
80-
p65
siRNA control
siRNA LKB1
siRNA LKB1 + p65
50-
LKB1
siRNA control
siRNA LKB1
siRNA LKB1 + p65
50-
β-tubulin

Figure 3E

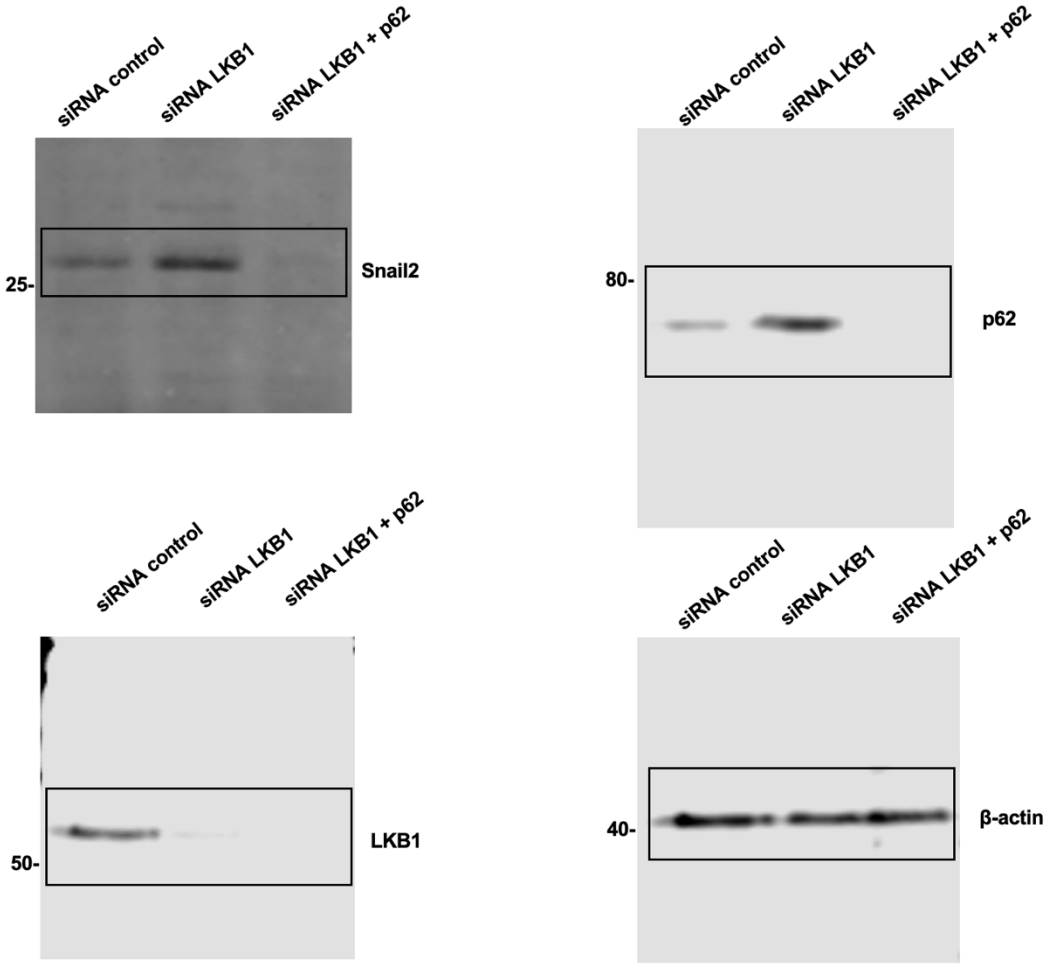
siRNA control
siRNA LKB1
siRNA LKB1 + p62
25-
Snail2
siRNA control
siRNA LKB1
siRNA LKB1 + p62
80-
p62
siRNA control
siRNA LKB1
siRNA LKB1 + p62
50-
LKB1
siRNA control
siRNA LKB1
siRNA LKB1 + p62
40-
β-actin

Figure 5F

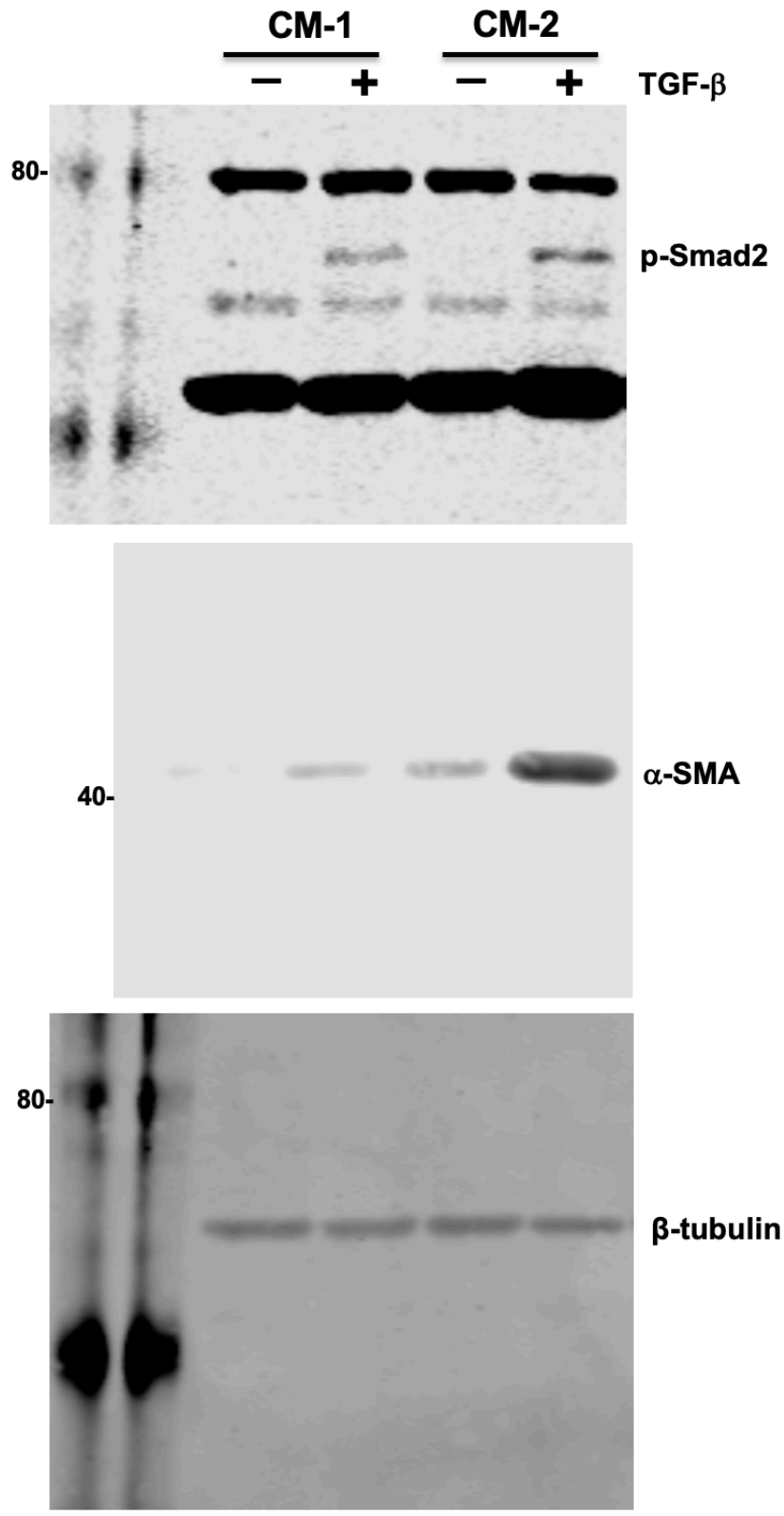

CM-1: control ATII CM
CM-2: LKB1-deplted ATII CM